INFLUENCING PROFIBROTIC MACROPHAGE POLARIZATION AND ACTIVITY USING YEAST-DERIVED MICROPARTICLES

TARGETING THE DECTIN-1 RECEPTOR VIA BETA-GLUCAN MICROPARTICLES TO MODULATE ALTERNATIVELY ACTIVATED MACROPHAGE ACTIVITY AND INHIBIT ALTERNATIVE ACTIVATION

By AARON IMRAN HAYAT, B.Sc. (Honours)

A Thesis Submitted to the School of Graduate Studies

in Partial Fulfillment of Requirements for the Degree

Master of Science

MASTER OF SCIENCE (2021) McMaster University
(Medical Sciences) Hamilton, Ontario

TITLE: Targeting The Dectin-1 Receptor via Beta-Glucan Microparticles to Modulate Alternatively Activated Macrophage Activity and Inhibit Alternative Activation

AUTHOR: Aaron Imran Hayat, B.Sc (Honours)

SUPERVISOR: Dr. Kjetil Ask, Ph.D

NUMBER OF PAGES: 83

ABSTRACT

Idiopathic Pulmonary Fibrosis (IPF) is a debilitating respiratory disorder that is s characterized by a progressive decline in lung function. Originating through unknown etiology, it is essentially an unchecked wound healing response that causes the build-up of excessive scar tissue in the lung interstitial tissue with a heavy toll on the patient's respiratory capacity. Pro-fibrotic alternatively activated macrophages (M2) have been linked as an important contributor to the fibrotic remodeling of the lung. Previous Ask research indicates that targeting M2 macrophages is possible through the use of the Dectin-1 receptor, a transmembrane cell surface receptor found in high abundance on M2 macrophages. Activating the Dectin-1 receptor through the use of beta-glucan, a ligand the receptor has a high affinity for, initiates a pro-inflammatory response within the naturally immunosuppressive macrophage and can alter its activity to be less fibrogenic.

Our data suggest that M2 polarization of naïve macrophages can be inhibited in vitro by beta-glucan microparticles. Additionally, we have found that polarized M2 macrophages adopt M1-like characteristics when treated with beta-glucan microparticles, in a process that is largely Dectin-1 dependent. M2 cell surface marker CD206, increased levels of which are associated with rapidly progressing IPF, shows significantly decreased frequency of expression in M2 macrophages treated with beta-glucan microparticles. Our assessment for cell-specific uptake of beta-glucan microparticles suggests an important role of the Dectin-1 receptor for significantly increased uptake in murine wild-type M2 macrophages relative to their Dectin-1 knockout counterpart.

The use of beta-glucan microparticles as a potential anti-fibrotic therapeutic was assessed in the bleomycin model of fibrotic lung disease. Mice given bleomycin and treated with beta-glucan displayed decreased soluble collagen content and TGFB expression within lung homogenate relative to fibrotic bleomycin control mice. Overall, these results provide insight into the use of beta-glucan as a potential activity modulator of macrophage function in IPF and the possibility of its use as a therapeutic.

ACKNOWLEDGMENT

Firstly, I'd like to praise and thank God for His blessings and for helping me through my studies. All of the work in this document would not have been possible without the support of my family. My parents have instilled in me a value system based on respect, resilience, empathy, and most importantly kindness. If not for their help and constant encouragement I would not have been able to do it. My siblings, Moses, Marry, and Adriel are wonderful and I'm grateful to them for always making me laugh. Ashini, thank you for all of your friendship, love, and support.

I feel very blessed to have been allowed to work at McMaster University and St. Joseph's Hospital for the past two years. I'd like to thank my supervisor Dr. Kjetil Ask for allowing me to be in his lab and work on this amazing project. Your patience and support have been crucial in the completion of my thesis. Your insights in everything from experimental designs to data interpretation laid the foundation of this work. Thank you for mentoring me and making my graduate studies a memorable experience.

I am sincerely grateful to my supervisory committee which has helped me tremendously throughout my graduate studies. Dr. Todd Hoare, you are genuinely an awesome mentor. Your continual faith in our collaborative work and the exceptional efforts you put forth in guiding us mentees is always reassuring. Dr. Anthony Rullo, you are the perfect mix of brilliance and kindness. In each of our interactions, you have taught me the importance of having mechanistic insight in my work and imparted a fascination with understanding why something works the way it does. Dr. Mark Larche, you are the gold standard of what a researcher needs to be. Your expertise in immunology and inquisitive questions have always motivated me to gain a deeper understanding of my work. I am immensely privileged to have been able to learn from all of you. The phrase "standing on the shoulders of giants" is an apt metaphor for what you all have done for me intellectually.

I express my gratitude towards Dr. Darren Bridegwater who I've had the pleasure of working with within the Demystifying Medicine Program, initiated by Dr. Ask. Dr. Bridgewater your care for students' learning experience and emphasis on making knowledge translation possible is motivating. Your efforts to make a friendly learning environment for all are what we should all aspire to do. Thank you for being the external examiner for this project.

My extended Ask Lab family has played a huge role in making this thesis possible. Dr. Olivia Mekhael and Megan Vierhout have been the most amazing friends I have made. Megan was my very first mentor at the Ask Lab and I wouldn't be here without her. Olivia, you have inadvertently played the role of the elder smarter sibling for me in the Ask Lab and taught me the technical skills I needed to be successful. Both of you have an immense propensity for compassion and a willingness to help others when they need it. I'd like to thank our new Master's candidates Vaishnavi Kumaran and Parichehr Yazdanshenas, you both have a bright future ahead of you and I wish you all

the success in your graduate studies. Spencer Revill and Amir Reihani have both played a crucial part in the histology work for this project and I am fortunate to have such dependable lab mates. Dr. Anmar Ayoub and Dr. Soumeya Abed have always been very kind to me and I am immensely appreciative of all that they have taught me. My earnest thanks go to Safaa Naiel and Li-Min Liu for the fun chats and their expertise in the animal work done for this project. You have all been a wonderful team to work with and I will always be grateful to you for giving me a unique graduate experience.

This project was funded primarily through the Collaborative Health Research Grant awarded to Dr. Ask, Dr. Hoare, and Dr. Brian Coombes, with Ceapro Inc. acting as the industry cohort. The entirety of the CHRP team deserves credit for helping shape this project from the start and they will hopefully be taking this research where it needs to go. Notably, Nate Dowdall from Dr. Hoare's team needs to be credited for his expertise in characterizing our compound(s) of interest and introducing the idea of macrophage "repolarization" to our team. Gilles Gagnon, Paul Moquin, and the rest of the Ceapro team have continuously put forth a passionate effort in this project. I am very happy to have worked with such endearing collaborators.

I am fortunate to have made some incredible friends throughout my Master's studies. I'd like to thank Mike Akan, Sudeshna Dhar, Alex Nobel, Mark Lychacz, Irfan Khan, Asfia Soomro, Quan Zhou, John Vrbensky, and the rest of the McMaster Medical Sciences Student Association. You all helped me enjoy the social experience of being a graduate student.

I have had tremendous support from the respective teams at the McMaster Immunology Research Center (MIRC) and the Firestone Institute for Respiratory Health (FIRH). Rebecca Turner, Eden Kapcan, Ben Lake, and the rest of the Rullo Lab have always been pleasant and I thank them for their camaraderie. Tom Mu from the Larche Lab and Fernando Botelho from the Richards Lab have both helped me develop my technical skills and I thank them for their willingness to teach. I am thankful to the faculty at both MIRC and FIRH for helping me develop my presentation skills and providing significant insights into my work.

Writing this acknowledgment statement has allowed me to reflect on the multitude of learning experiences I've had since the start of my studies. It hasn't always been easy, but I am ever more appreciative of the experiences and the growth as a researcher.

TABLE OF CONTENTS

LIST OF FIGURES

LIST OF ABBREVIATIONS

α-SMA	Alpha Smooth Muscle Actin
AAM	Alternatively Activated Macrophage
BMDM	Bone-Marrow Derived Macrophage
CCl18	Chemokine ligand 18
ELISA	Enzyme Linked Immunosorbent Assay
ER	Endoplasmic reticulum
ECM	Extracellular Matrix
FEV1	Forced expiratory volume in 1 second
FFPE	Formalin-fixed paraffin-embedded
FVC	Forced vital capacity
H&E	Hematoxylin and eosin
IHC	Immunohistochemistry
IL	Interleukin
ILD	Interstitial lung disease
IPF	Idiopathic pulmonary fibrosis
LPS	Lipopolysaccharide
M1	Classically activated macrophage phenotype
M2	Alternatively activated macrophage phenotype
MCSF	Macrophage Colony Stimulating Factor
PMA	Phorbol Myristate Acetate
TMA	Tissue microarray
UPR	Unfolded protein response
TGF-β	Transforming growth factor beta
TLR	Toll Like Receptor
TMA	Tissue microarray

DECLARATION OF ACADEMIC ACHIEVEMENT

This is a declaration that the work presented in this thesis was completed by Aaron Imran Hayat, under the supervision of Dr. Kjetil Ask. Flow cytometry staining and analysis were performed by Dr. Olivia Mekhael. TMA generation was done at the Molecular Phenotyping and Imaging Core facility by Amir Reihani, with slide digitalization and staining quantification by Spencer D. Revill. Tolerability studies for beta-glucan microparticles in diseased (bleomycin) and naïve mice were done in conjunction with fellow Ask Lab members Safaa Naiel and Limin Liu.

INTRODUCTION

ILDs and IPF

Fibroproliferative disorders are a leading cause of morbidity and mortality worldwide (T. A. Wynn, 2004). Pulmonary inflammation and fibrosis form common endpoint pathways of interstitial lung disease (ILD) pathogenesis (Wynn, 2004). Idiopathic Pulmonary Fibrosis (IPF) is a major type of ILD and is characterized by a progressive decline in lung function. Presently, there are no effective treatments and median survival is between 3-5 years after diagnosis (Park & Lee, 2013). It has been stipulated that chronic inflammation of the lung is an important precursor to the onset of fibrosis (Wei et al., 2013; Glifford et al., 2012). Hallmarks of IPF are the fibrotic remodeling of the lung and excessive extracellular matrix deposition (Ask et al., 2006).

Characterized as restrictive lung disease (RLD), IPF impedes respiratory mechanics by increasing lung stiffness, causing dyspnea, and making it harder for patients to breathe (Gross & Hunninghake, 2001; Kalchiem-Dekel et al., 2018). Histopathologic analysis of IPF lung biopsies demonstrates usual interstitial pneumonia (UIP), showing a honeycombing pattern with or without peripheral traction bronchiectasis (Raghu et al., 2018; Sgalla et al., 2019). There is no one cause associated with IPF, rather damage from a host of depreciatory environmental stimuli, infections, physical injury, and autoimmune reactions are some possible avenues for IPF onset (Wynn, 2004). Repeated damage to epithelial tissue leads to the development of fibrosis downstream, with endoplasmic

reticulum (ER) stress and the unfolded protein response (UPR) playing an important role (Wei et al., 2013).

IPF Immunopathogenesis & UPR

Fibrotic lung disease progresses via an aberrant or unchecked wound healing response that occurs within pulmonary tissue (Ask et al., 2006). The exact initiation of the fibrogenic process as it pertains to IPF is quite a nuanced topic. Repeated micro-injuries, often caused by any one of a host of environmental insults, cause a chronic inflammatory response that triggers massive immunosuppression and exacerbated injury repair in lung tissue (Ask et al., 2006; Desai et al., 2018; Wei et al., 2013). The exact pathogenesis of IPF is poorly understood, hence creating targeted drug therapies remains a major hurdle. Important to the presentation of fibrosis is the accumulation of myofibroblasts as they are involved in the synthesis and deposition of ECM (Coward et al., 2010). It is, therefore, worthwhile to explore how myofibroblasts are stimulated and accumulate in lung tissue. It is well known that macrophages regulate myofibroblast activity but the exact mechanism of this process is complicated to determine (T. Wynn & Barron, 2010). It is difficult to understand fibrosis regulation as it is a heterogeneous process with multiple factors playing a key role.

Treatments that target the chronic inflammatory response produced during IPF have failed to garner effective results (Ask et al., 2006). Anti-inflammatory therapies, including corticosteroids used to treat nephrotic disorders, are of no significant benefit (Gibbons et al., 2011). Accordingly, research methods have shifted from treating chronic

inflammation to impaired wound healing and aberrant injury repair (Ask et al., 2006). This makes sense as using anti-inflammatory therapies does not impact the fibrotic remodeling process, therefore the problem must be that the injury repair response must be continuing unchecked. Ongoing research at the Ask lab looks to evaluate the role of protein misfolding (due to chronic respiratory stress as seen in IPF) and how it can contribute to the fibrotic process. Proteins are involved in a variety of cell processes that are essential to cellular function, meaning their synthesis, folding, and adequate degradation is key (Wei et al., 2013). The rough endoplasmic reticulum (ER) is responsible for the folding and posttranslational modifications of about a third of cellular proteins (Wei et al., 2013). The ER can become stressed due to injuries to tissues, and this can impact protein folding mechanisms. ER stress in the lungs can cause protein misfolding in alveolar epithelial cells (ACEs) and this has been linked to sporadic IPF pathogenesis (Tanjore et al., 2012). UPR mechanisms improve protein folding, maintain cellular homeostasis, and prevent apoptosis from misfolded protein accumulation (Tanjore et al., 2012). If the UPR mechanism fails in cases of ongoing ER stress, it can lead to cell death. ER stress and the UPR can lead to physiologic changes in the cell, like transforming growth factor-beta (TGF-B) expression, myofibroblast differentiation, epithelial-mesenchymal transition (EMT), and apoptosis (Wei et al., 2013). Studies show that AECs in areas of fibrosis in IPF had ER stress, it has been suggested that epithelial cells in the lungs contribute to fibrosis by changing to an (EMT) mesenchymal cell type (Tanjore et al., 2012). This provides evidence that ER stress may lead to fibrotic AEC incidence through EMT.

How chronic ER stress leads to the appearance of fibrosis is best understood through myofibroblast function. Myofibroblasts have a high profibrotic potential which is the reason they are the primary depositors of ECM and are involved in the lung's deteriorating architecture (Park & Lee, 2013). Fibroblasts differentiate into myofibroblasts in the lung due to mechanical stress, increased TGF-B presence, and various matrix proteins among other components (Park & Lee, 2013). Macrophages also seem to play an important role but the direct interaction is unknown. Myofibroblasts induce excessive accumulation of extracellular matrix, breakdown of membranes, and epithelial cell death (Park & Lee, 2013). The organization of the ECM is a major influencer of fibrosis onset, with the presence of various factors playing a key role (Glifford et al., 2012). Factors like cytokines, kinases, MMPs, chemokine, various collagen types, PDGF, and TGF-B have a profound impact on the maintenance of elasticity and ACE integrity (Glifford et al., 2012). The TGF-B1 cytokine is known to be a profibrotic factor in IPF and other fibrotic diseases (Wynn & Barron, 2010). Elevated TGF-B levels are seen in bronchoalveolar lavage fluid (BALF) and lung tissue from IPF patients (Glifford et al., 2012). TGF-B allows for myofibroblast differentiation, ECM production, and inhibits matrix degradation (Ask et al., 2006).

IPF Medications

Currently, pirfenidone and nintedanib are two FDA-approved drugs used to treat IPF. With TGF-B as a potential therapeutic target, studies have attempted to block it in mice and humans (Fernandez & Eickelberg, 2012). Pirfenidone proves to exhibit

antifibrotic and anti-inflammatory effects by reducing TGF-B expression (Fernandez & Eickelberg, 2012). It is worthwhile to note that the key benefit of pirfenidone therapy is a slower decline in lung function, measured through forced vital capacity (FVC), and it is not a permanent solution (Fernandez & Eickelberg, 2012). A significant reduction in disease progression, death, and dyspnea is seen in patients treated with pirfenidone relative to the placebo group (Somogyi et al., 2019). Nintedanib, a tyrosine kinase inhibitor, also shows antifibrotic effects by inhibiting fibroblast proliferation and differentiation (Wollin et al., 2015). Phase II and III clinical trials for nintedanib have shown a slower decline in FVC, even for patients with an advanced disease profile (Somogyi et al., 2019). Nintedanib inhibits multiple tyrosine kinases including PDGF, VEGF, and FGF (Bonella et al., 2015). The exact mechanism by which pirfenidone and nintedanib exert anti-fibrotic effects is still unknown, and it seems that these effects are non-permanent..

There are a plethora of next-generation drugs currently in development for IPF treatment as the need for cell-specific drug delivery is vital (Abed et al., 2021; Somogyo et al., 2019). There are significant systemic side effects associated with nintedanib and pirfenidone such as nausea, headaches, diarrhea, and vomiting among others (Chen et al., 2021; Lancaster et al., 2017). Cell-specific drug targeting can potentially reduce uncomfortable systemic side effects and accordingly be more effective in treatment.

Macrophages in Fibrosis

Macrophages are traditionally known as cells that phagocytose and clear away cellular debris/pathogens via phagocytosis. Macrophages promote or slow the progression of fibrosis, depending on the type of dead cells that are being engulfed and removed (Wynn and Barron, 2010). Macrophages repress inflammation when clearing away apoptotic cells and promote inflammation during necrotic cell removal (Wynn and Barron, 2010). TGF-B1 secretion by macrophages occurs during cell removal, making the process profibrotic but removing dead myofibroblasts, hepatocytes, and cellular debris can eliminate TGF-B1 and other profibrotic cytokines (Wynn and Barron, 2010). Macrophages produce other profibrotic factors like platelet-derived growth factor (PDGF) and regulate the ECM levels of metalloproteinases (Wynn & Barron, 2010). Macrophages and the factors they express are present throughout the fibrotic process. It has been proposed that collagen-secreting myofibroblasts produce the fibrotic phenotype, while macrophages regulate it (Wynn and Barron, 2010).

Traditionally, macrophages are divided into either a pro-inflammatory or M1 (classically activated) phenotype or a pro-fibrotic or M2 (alternatively activated) phenotype, however, this distinction is more clearly seen *in vitro* (Murray & Wynn, 2011). It is important to understand that macrophage phenotypes are rather plastic, with the ability to be polarized by stimuli in the cells' microenvironment (Braga, Agudelo, & Camara, 2015). There have been *in vivo* studies that suggest that macrophage phenotypes lie on a wide spectrum, with macrophages capable of exhibiting M1 and M2 qualities in tandem (Sica & Mantovani, 2012). Specifically, through *in vitro* studies, undifferentiated macrophages can be polarized to the M1 phenotype through interferon-gamma (IFN-γ)

and bacterial lipopolysaccharide (LPS) exposure, while the M2 macrophage can be polarized by stimulating naïve macrophages with the cytokines IL-4 and IL-13 (Weischenfeldt & Porse, 2008). A hyperpolarized M2 macrophage can be obtained by adding IL-6 to a profibrotic cocktail containing IL-4 and IL-13 (Ayaub et al., 2017).

An immune response is typically started with an inflammatory response where M1 macrophages are in majority and increase their rate of phagocytosis and produce proinflammatory cytokines like TNF-α, IL-12, IL-1B, and IL-23 (Braga, Agudelo, & Camara, 2015). This is followed by a wounding healing/tissue repair response where M2 macrophages produce anti-inflammatory cytokines such as IL-10 to resolve inflammation along with pro-fibrotic factors like TGF-β (Wynn & Vannella, 2016). TGF-B has been known to cause fibroblasts, epithelial cells, and progenitor cells to enable the wound healing response to restore the structural integrity of healthy tissue after an inflammatory response (Wynn & Vannella, 2016). When the tissue repair response becomes aberrant, the excretion of unnecessary profibrotic factors in the ECM can result in the fibrotic remodeling of the lung (Wynn & Vannella, 2016). Based on this it makes sense to specifically target M2 macrophages to prevent the progression of fibrosis.

Gibbons et al., explain that the role of monocytes or macrophages in the pathogenesis of pulmonary fibrosis is uncertain, but that alternatively activated (M2) macrophages may be profibrotic (2011). The Gibbons et al. study showed the importance of circulating monocytes and lung macrophages during pulmonary fibrosis and emphasize the importance of the alternatively activated macrophage phenotype. The study results showed that Ly6Chi monocytes facilitate the progression of pulmonary fibrosis after

being transferred in mice (Gibbons et al., 2011). Interestingly, after the adoptive transfer of monocytes into mice along with a bleomycin insult showed increased fibrosis and M2 macrophages (Gibbons et al., 2011). Prominent cell surface markers associated with M2 macrophages are CD206, CD163, CD200R membrane glycoprotein, as well as proteins like arginase-1, MMR, FIZZ1, and Ym1 in the murine model (Abed et al., 2021).

Strategies that look to reprogram profibrotic macrophages into antifibrotic macrophages are a possible option to suppressing fibrosis. Folate targeted TLR7 agonists have been used to suppress profibrotic macrophage activity within the bleomycin model of fibrotic lung disease in mice, resulting in decreased profibrotic cytokine release, collagen deposition, and overall fibrotic phenotype as determined by histology (Zhang et al., 2020). We too are interested in reprogramming M2 or profibrotic macrophages by cell-specific drug targeting. Using a bioinformatics approach, the Ask Lab has identified Dectin-1/Clec7a to be a unique marker for M2 macrophages (Patel, 2018). Increased understanding and characterization of this pathway will clarify the role of Dectin-1 activation in macrophages associated with fibrotic lung disease and potentially allow it to be a biological target that could aid in preventing the progression of fibrotic lung disease.

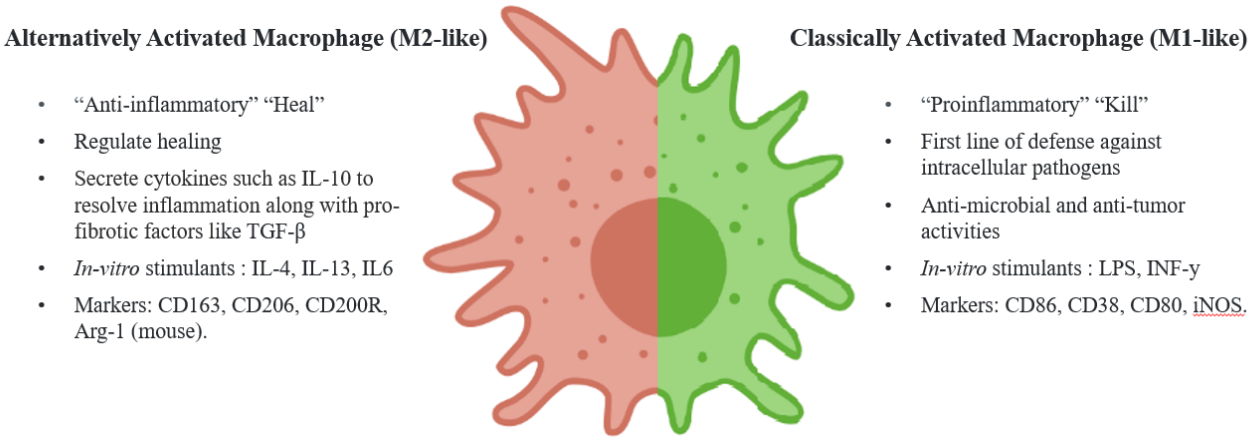

Created with BioRender.com

Figure 1: Macrophage Heterogeneity in Immune Responses

Macrophages can adopt M2 or M1-like characteristics based on environmental stimuli to aid in innate immune responses related to either inflammation or wound repair. They correspondingly express distinct surface markers and initiate apt cytokine production to aid in their function.

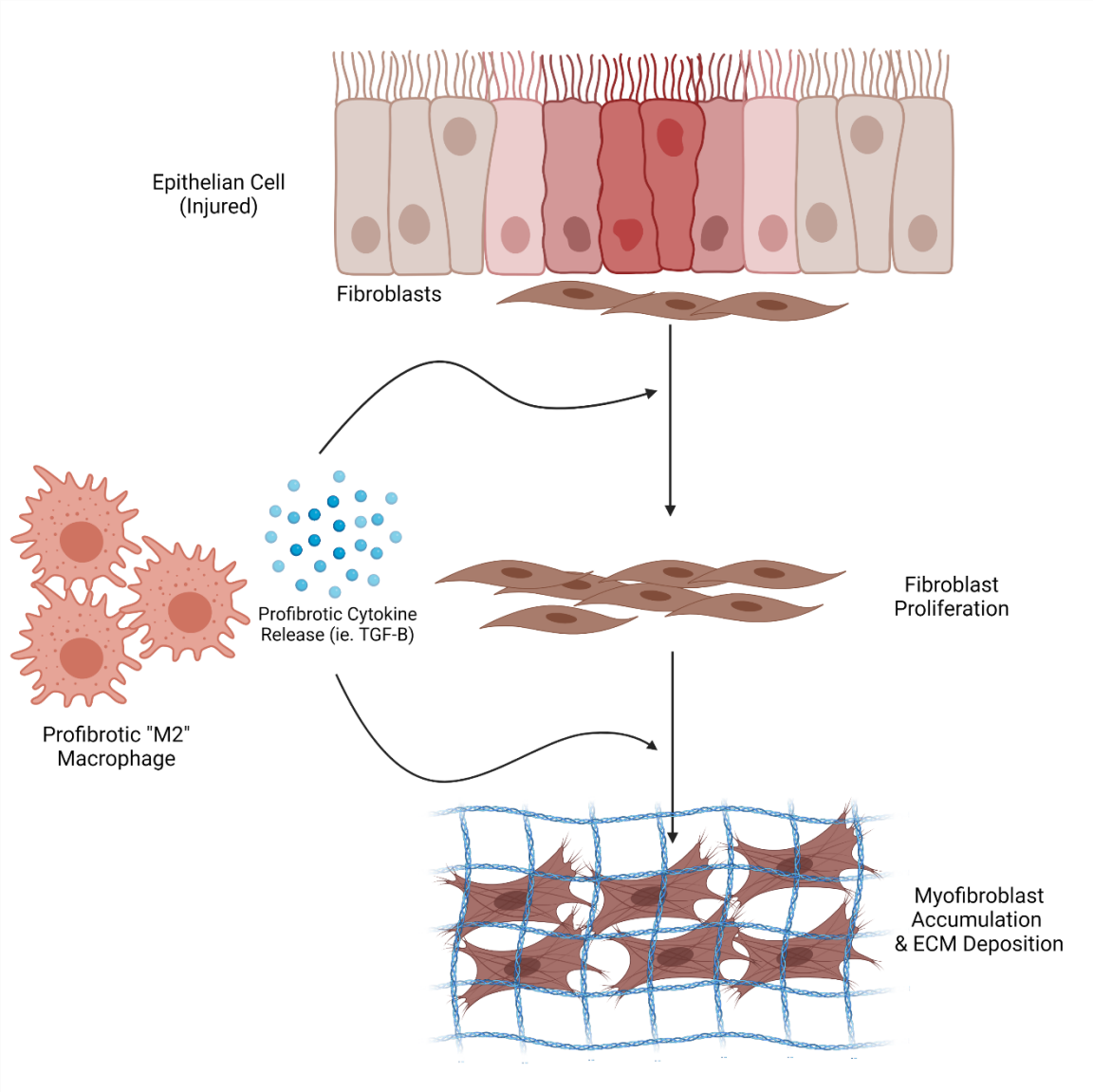

Created with BioRender.com

Figure 2: Profibrotic Macrophages as Regulators of Fibrosis

Profibrotic “M2” macrophages contribute to the fibrotic remodeling of tissue post tissue injury. Profibrotic cytokines released by M2 macrophages like TGF-B cause differentiation of fibroblasts to myofibroblasts and ensuing ECM deposition.

Dectin-1 Receptor & Spleen Tyrosine Kinase (SYK) Pathway

Dendritic-cell (DC)-specific receptor (Dectin-1) is expressed by the human C-type lectin domain family 7 member A (Clec7a) gene on chromosome 12 (Brown, 2006). It was originally believed to be expressed on DCs alone; however, it was later found to be expressed in numerous cell types, including monocytes, macrophages, neutrophils, and even T-cells (Willcocks et al., 2006). Known to bind b-1,3 and with greater affinity relative to b-1,6 linked glucans, Dectin-1 is a non-TLR with a critical role in identifying fungal invasion (Brown, 2006). Upon ligand binding, dectin-1 initiates phagocytosis and an inflammatory response; however, dectin-1 is also recognized as a co-stimulatory molecule that can bind CD4+ and CD8+ T-cells *in vitro*, suggesting it may assist in T-cell activation (Brown et al., 2007). Deduced from its primary structure, Dectin-1 is a 28kDa receptor with three major components (Brown et al., 2007). In the extracellular domain, it contains a C-type lectin-like domain, the CRD, in which further studies found six Cys residues to be highly conserved among C-type lectins (Brown et al., 2007). The extracellular domain is connected to a transmembrane region via a stalk that lacks Cys residues, indicating that the receptor can act as a monomer and does not require downstream dimerization (Brown, 2006). Finally, an immunoreceptor tyrosine-based activation motif (ITAM)-like motif, referred to as hemITAM, lies in its cytoplasmic domain (Borwn et al., 2007). ITAMs contain repeated YXXI/L (Tyrosine-X-X-Isoleucine/Leucine) amino acid sequences in which the tyrosine is phosphorylated by members of the SRC tyrosine kinase family (Brown et al., 2007). Upon ligation of β-glucan, Dectin-1 recruits the adaptor protein CARD9 to phosphorylate spleen tyrosine

kinase (Syk) which in turn initiates a signaling cascade that induces phagocytosis and leads to the activation of nuclear factor-κB (NF-κB) and MAPK (Kimura et al., 2014).

Translational findings were provided by Liu et al. in which repolarization of tumor-associated macrophages (TAM) from an alternatively-activated phenotype back to an M1-like phenotype was made possible via b-glucan administration (2015). Macrophages in a tumor setting referred to as TAM, have been heavily correlated with the M2 phenotype, verified through the expression of arginase-1, vascular endothelial growth factor, and PGE2 (Liu et al., 2015). The M2 phenotype plays a critical role in the tumor-promoting activity, allowing immune evasion given that the M1 activation is switched to an M2 activation early in tumor activation (Liu et al., 2015). In addition, evidence exists that M2 TAMs limit the efficacy of chemotherapeutic agents, emphasizing its ability to serve as an immunotherapeutic target for cancer therapy (Liu et al., 2015). Upon *in vitro* addition of whole glucan particle to M2-like TAM macrophages, downregulation of M2 marker genes and upregulation of M1 marker genes were observed (Liu et al., 2015).

Dectin-1 Targeted Drug Delivery

In collaboration with the Hoare lab and Ceapro Inc., we aimed to test the use of beta-glucan microparticles and how they can influence M2 macrophage polarization. Making use of Ceapro's processing technology and the Hoare lab's ability to characterize these microparticles we were able to obtain a variety of different beta-glucan microparticles for source, size, chemical characteristics, and processing. The eventual

development of appropriate inhaled therapeutic strategies offers the potential to both increases the level of drug reaching the affected areas of the lung as well as limit potential side-effects by reducing the amount of drug-exposed systemically. The highly porous beta-glucan microparticles produced via PGX (pressurized gas expanded liquids technique developed by Ceapro) offer unique potential benefits in this context given their low density (allowing for deeper lung penetration), small size (improved retention and increased macrophage phagocytosis), and high capacity for loading nintedanib. Given beta-glucans binding affinity to the Dectin-1 receptor, loading beta-glucan microparticles with nintedanib offers an opportunity to get targeted delivery of the drug to its target fibrotic macrophages in the lung. We know that the Dectin-1/SYK pathway activation is important in regulating inflammatory responses within an M2 macrophage and want to explore how well Ceapro's processed beta-glucans can do this relative to non-PGX controls. Table 1 below lists the different beta-glucans we have tested along with their known characteristics. PGX yeast beta-glucan also referred to as 20F17, is the primary microparticle we are interested in due to its small size (relative to the cell membrane) and abundance of B-1,3 glycosidic linkages that the Detin-1 receptor has a high affinity for.

Table 1: Beta-glucan Varieties Tested in Macrophage Polarization Experiments

Name	Abbreviation	Glycosidic Linkage(s)	Size	Source	Solubility in water
Non-PGX Yeast beta-glucan	YBG	B-1,3	< 100 μm	Ceapro Inc.	No

PGX yeast Beta-glucan	20F17	B-1,3	1-10 μm	Ceapro Inc.	No
PGX oat beta-glucan	OBG	Mixed B-1,3 and B-1,4	< 100 μm	Ceapro Inc. (biopolymer)	Yes
Zymosan	Zymo	B-1,3	3 μm	ThermoFisher Scientific (Cat#Z2849)	No
PGX Nintedanib impregnated yeast beta-glucan	NTB-YBG	B-1,3	< 100 μm	Ceapro Inc.	No

Hypothesis

I hypothesize that PGX beta-glucan (20F17) microparticles can modulate polarized M2 macrophage activity as well as inhibit M2 polarization in a Dectin-1 dependent manner. To address this hypothesis, I will investigate the polarization of murine bone-marrow and human THP-1 monocyte-derived macrophages *in-vitro* when co-treated with 20F17 and an anti-inflammatory cocktail (IL-4, IL-13, IL-6), as well as treatment of polarized M2 cells with 20F17. Further, as our lab has previously shown that M2 macrophages have a more abundant expression of Dectin-1, I hypothesize that polarized M2 macrophages will uptake 20F17 to a higher degree relative to naïve macrophages. Lastly, it is pertinent to assess how 20F17 and nintedanib-loaded yeast-beta glucan (NTB-YGB) microparticles can serve as an antifibrotic therapeutic. Accordingly, I hypothesize that mice given 20F17 and NTB-YBG at day 7 and day 14 in the bleomycin

model of fibrotic lung disease will show decreased fibrotic outcomes, relative to untreated mice given 0.05U of bleomycin.

Objectives

Objective 1: Assess M2 macrophage polarization in the presence of beta-glucan microparticles

To determine the effect of 20F17 and other beta-glucan microparticles on M2 macrophage polarization it is important to utilize the M2 polarization assay as previously shown in our lab by Ayaub et al (2017). In this assay, an anti-inflammatory cocktail containing IL-4 (20ng/ml), Il-13 (50 ng/ml), and IL-6 (5ng/ml) can transition naïve macrophages to a hyperpolarized M2 state, as assessed by elevated arginase-1 activity in murine bone-marrow-derived macrophages (BMDMs) and CCl18 production in human monocyte-derived THP-1 macrophages (Ayaub et al., 2017). Referring to Liu et al.'s study, treating polarized TAM M2-like macrophages with 100 ug/ml of beta-glucan skews these macrophages to an M1-like phenotype via a Dectin-1 mediated inflammatory response (2015). Other than examining whether a dose-dependent response exists, there are two key questions related to M2 polarization and how beta-glucan microparticles can affect it. Namely, we are interested in how a co-treatment with the M2 cocktail and our microparticles affects polarization, and what effect can be seen when the microparticle treatment occurs after M2 polarization has occurred (24 hours of cytokines treatment followed by 24 hours of microparticle treatment). Both lines of investigation are relevant because there are different macrophage populations in the lung. There are resident

alveolar and interstitial macrophages that are terminally differentiated and have an M2-like subset involved in wound healing processes, as well as macrophages derived through circulation from monocytes that can transition into the M2-like state (Chavez-Galan et al., 2015). Therefore, it becomes relevant to assess how microparticles have the potential to modulate activity in M2 polarized cells as well as inhibit polarization in naive macrophages.

To undertake this objective, we set up two different types of M2 polarization assays, the co-treatment angle, and the polarized angle. In the co-treatment angle, we tested how naïve macrophages (BMDM and THP-1) when treated with the M2 cocktail and beta-glucan concurrently, express M2 markers after 24 hours of treatment. The main assessment tool used in murine BMDMs was the arginase-1 assay and CD206 expression via flow cytometry. Arginase-1 is a reliable M2 macrophage marker and is seen in increased levels with our M2 cocktail (Ayaub et al., 2017). Arginase-1 is relevant in the murine fibrotic models as it contributes to the severity of fibrogenesis, as shown previously in the murine silica model (Dias et al., 2015). CD206 has been shown as an important biomarker for IPF as elevated soluble CD206 levels have been associated with mortality (Zou et al., 2020). Relevant to THP-1 macrophages, CCL18 is a well-characterized marker for M2 polarization that has clinical importance as well. CCl18 expression by M2-like macrophages is directly involved in initiating collagen production by fibroblasts and furthers fibrogenesis (Prasse et al., 2006). The assessment techniques for M2 polarization are the arginase-1 assay for BMDMs, CCL18 ELISA, as well as flow

cytometry for CD206 expression. The use of Dectin-1 knock-out (KO) BMDMs will serve as a negative control.

Assessing any possible cytotoxicity these microparticles have with macrophages becomes a topic of contention as any changes picked up in our functional assays should not be due to cell death. We used a lactate dehydrogenase (LDH) assay to determine beta-glucan mediated cytotoxicity in macrophages relative to the lysed control. LDH is a suitable indicator of cell viability since it leaks into the cellular environment from the cytoplasm after cellular damage occurs and can be correlated with toxicity (Kaja et al., 2017).

To gain mechanistic insight into how M2 macrophages adopt M1-like characteristics post-beta-glucan treatment we will assess TNFa and nitric oxide (NO) production in our wildtype and Dectin-1 KO macrophage models. TNFa and NO are reliable proinflammatory indicators we can use to ascertain whether macrophage reprogramming occurs at the cellular level.

Objective 2: Examine uptake of labeled microparticles by macrophages in a phagocytosis assay

Cell-specific uptake of beta-glucan microparticles is a key aim as we have demonstrated in the past that the Dectin-1 receptor is specifically expressed on the M2 phenotype. Since beta-glucan is the ligand for the dectin-1 receptor, the phagocytic rate of beta-glucan microparticles should be higher in the M2 phenotype. This aim requires a specific design where beta-glucan microparticles (20F17 has a size distribution of 1 – 10

microns) will need to be fluorescently labeled with a dye (aniline blue). Past studies have used red-dyed zymosan particles (peak fluorescence at OD of 540 to 570 nm) to assess phagocytosis in macrophage cell lysates (Roedel et al., 2012). Wild-type (expressing dectin-1) and full body dectin-1 knock-out mice (KO will serve as negative controls) can be used to obtain naive BMDMs. Naïve BMDMs and THP-1 macrophages will be polarized in-vitro to the M2-like phenotype and then treated with the fluorescently dyed beta-glucans (concentration of 100 ug/ml and 10 ug/ml with no-treatment controls) for 1 to 6 hours, a period obtained from past phagocytosis studies (Kapellos et al., 2016; Roedel et al., 2012). Aniline Blue was used as the fluorescent dye to tag the microparticles. With beta-glucan uptake being assessed through a fluorescent plate reader and visualized using a fluorescent microscope.

Objective 3: Evaluate the use of 20F17/NTB-YBG microparticles as anti-fibrotic therapeutics in the bleomycin model of fibrotic lung disease

Assessing the efficacy of PGX microparticles is essential as we want this vehicle/drug delivery method to prevent fibrosis in an *in vivo* model for the overall goal of translational research in humans. Although the bleomycin model does not recapitulate all the features of human fibrotic lung disease, it is a good model to use (Moeller et al., 2008). Bleomycin has been used as a medicinal agent in chemotherapy but also causes an overproduction of reactive oxygen species which leads to an inflammatory response and fibrosis (Moeller et al., 2008). The initial inflammatory response to bleomycin is followed by a switch to fibrosis, approximately 14 days after intratracheal administration (Moeller et al., 2008). The time course of the bleomycin model is as follows: baseline at day 0,

inflammatory and injury phase at day 7, the fibrotic phase at day 14, and resolution phase at day 28 (Pitozzi et al., 2018). Bleomycin-induced fibrosis produces human-IPF features such as intra-alveolar buds, mural incorporation of collagen, and obliteration of the alveolar space in mice (Moeller et al., 2008). The fact that this model produces features of human disease in animals makes it a reliable and popular model to use.

Here we exposed female 11-12-week old wild-type C57Bl6/J mice to bleomycin (0.05U per mouse in 50 ul saline) via oral-pharyngeal intubation under inhalable anesthesia. Eight groups (n=4/5) were set up to assess anti-fibrotic efficacy, namely, 1) 0.9% NaCl saline group, 2) bleomycin fibrotic control, 3) 20 ug 20F17 given at Day 7, 4) 20 ug 20F17 given at Day 7 and 14, 5) 2 ug 20F17 given at Day 7, 6) 2 ug 20F17 given at Day 7 and Day 14, 7) 2 ug NTB-YBG given at Day 7, 8) 2 ug NTB-YBG given at Day 7 and Day 14. This experiment allowed us to demonstrate the therapeutic efficacy of our microparticles as antifibrotic agents in the bleomycin model. We also tested the time of intervention (Day 7 vs Day 14), the dose required (high dose = 20 ug, low dose = 2 ug), and frequency of treatment. After conducting microparticle tolerability studies in naïve mice and mice that were given bleomycin, we know that beta-glucan microparticles have a significant immune modulatory effect, resulting in short-term pulmonary inflammation. Doses higher than 20 ug per mouse are not desirable as they can initiate an excessive inflammatory response within the lung. Previously, the 20 ug dose of beta-glucan has been tested with bleomycin-induced lung fibrosis in rats (oral gavage being the method of treatment) and results indicated a protective effect when the treatment was started 12 hours after bleomycin intubation (Iraz et al., 2015). Therefore, we tested the same dose in

mice as our high dose, and 2 ug as the low dose, which seems to be highly tolerable in naive and diseased mice. Nintedanib-loading on PGX-YBG particles has been quantified by the Hoare lab as 0.5% approximately. Given how 50nM of nintedanib per animal per 24-hour period has been used in prior studies (Epstein-Shochet et al., 2020), the 2 ug dose for the NTB-YBG provides 0.01855 nM nintedanib. In line with our hypothesis, we hope to show that beta-glucan microparticle treatment is protective against fibrotic outcomes and lowers the prevalence of M2 macrophages at Day 21 in mice treated with our microparticles relative to untreated mice. We generated a tissue microarray (TMA) block using mouse left lobe tissues for staining with H&E, Masson's Trichrome for collagen assessment, and immunohistochemistry (IHC) staining for CD206 as the M2 macrophage marker and pSYK. Outcomes like tissue histology, measurement of the soluble collagen content in the lungs, and cytokine assessment in the BAL and lung homogenate serve as the primary readouts for this aim.

METHODS

Bone Marrow-Derived Macrophage Isolation and Culture

Bone marrow-derived macrophages (BMDMs) were isolated and cultured from wildtype C57BL6/J mice and Dectin-1/Clec7A KO mice aged-matched at 8-10 weeks. Bone marrow cells were extracted from the mouse tibia, femur, hip, and spine as previously described (Ayaub et al., 2017). Extracted bone marrow cells were treated with 20 ng/ml of recombinant mouse M-CSF (macrophage colony-stimulating factor) for 7 days. Media used was DMEM/F12 (10% FBS, 1% pen/strep, 1% glutamine), supplemented with M-CSF (PeproTech, Cat# 315-02). After 7 days, the resulting bone marrow-derived macrophages (M0 -naive) were lifted off of culture plates using Accutase cell dissociation reagent (ThermoFisher catalog number A1110501) and seeded in a 96-well plate at a density of 80 000 cells per well, or in a 60 mm culture dish at a density of 5 million cells per plate for flow cytometry experiments (treatment volume being 100 ul in the 96-well plate and 3 ml in the 60 mm petri dish).

To obtain hyperpolarized M2 macrophages an anti-inflammatory cytokine cocktail comprised of mouse recombinant IL-4 (20 ng/ml; Cedarlane catalog # D-61409-20UG), IL-13 (50 ng/ml; Cedarlane catalog # D-62312-10UG), and IL-6 (5ng/ml; Cedarlane catalog # 216-16-10UG) was used as described previously (Ayaub et al., 2017). To obtain M1 macrophages a pro-inflammatory cytokine cocktail of lipopolysaccharide (LPS; 100ng/ml; Sigma catalog # 82857-67-8) and interferon-gamma (IFNγ; 10ug/ml; ThermoFisher catalog number PMC4031).

For co-treatment experiments, beta-glucan microparticles (1000 ug/ml to 1 ug/ml) and the anti-inflammatory cytokine cocktail were introduced to naïve macrophages simultaneously for 24 hours. For polarized macrophage experiments cells were treated with the anti-inflammatory cocktail for 24 hours first and then treated with beta-glucan microparticles for an additional 24 hours.

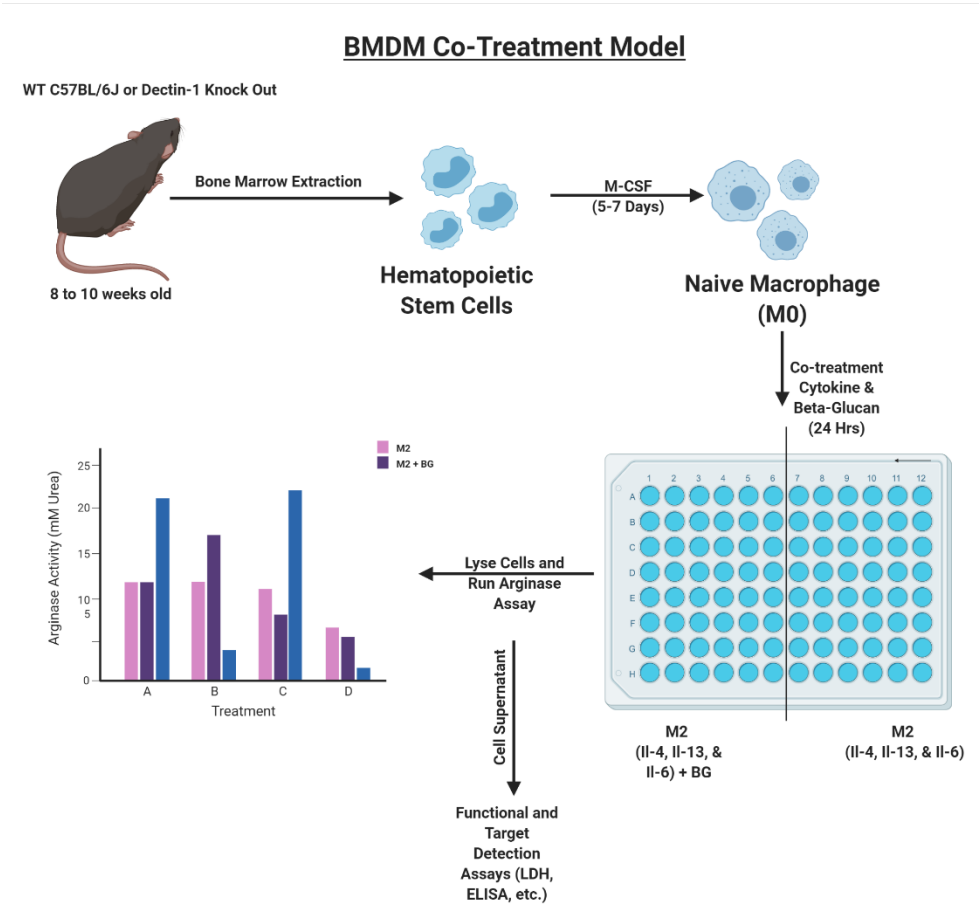

Created with BioRender.com

Figure 3: BMDM Co-Treatment Model

M2 macrophage polarization in the presence of beta-glucan microparticles was tested using the arginase-1 assay as suggested by the above workflow. Cell supernatant was stored for downstream testing.

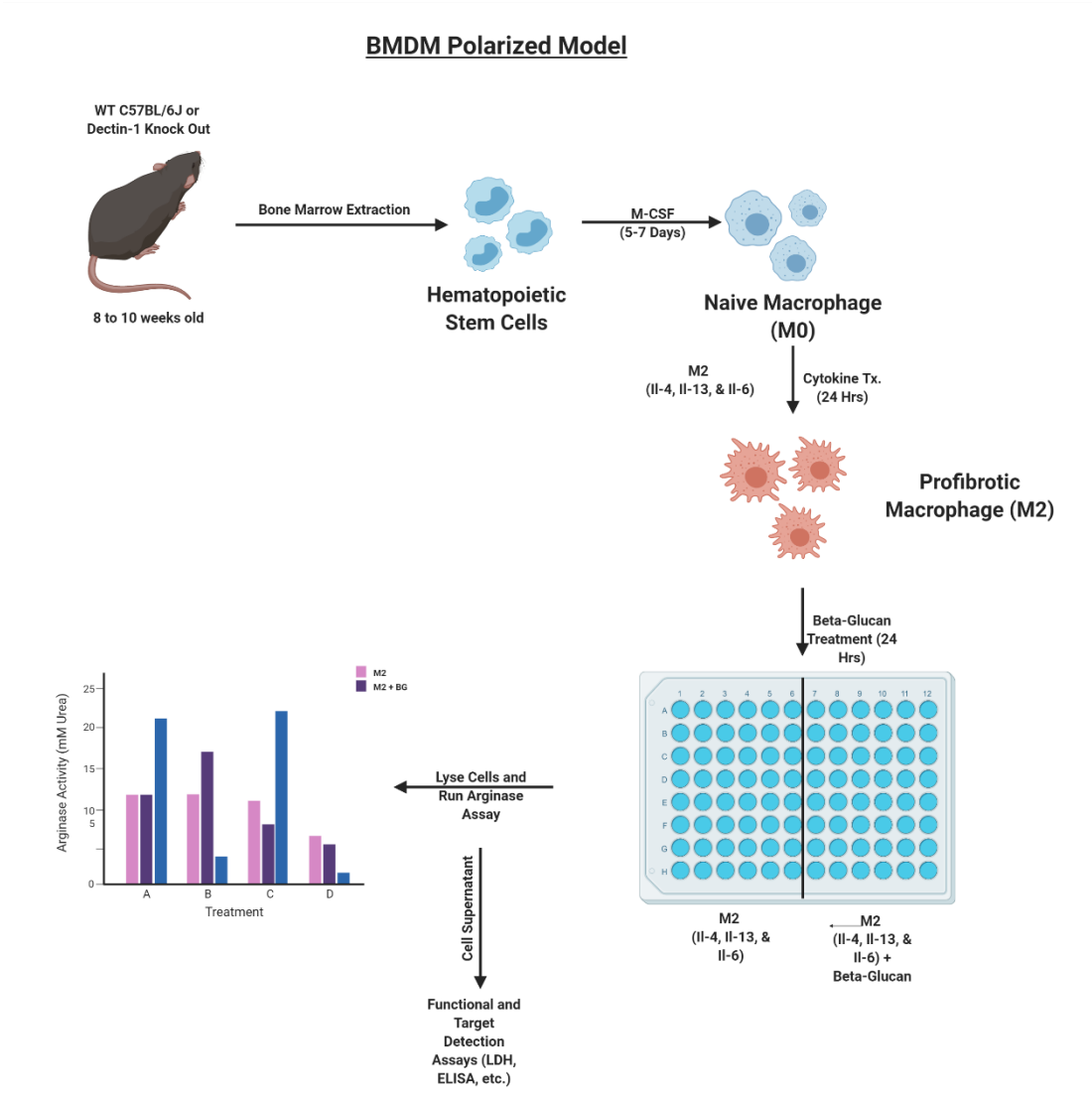

Created with BioRender.com

Figure 4: BMDM Polarized Treatment Model

Macrophages were polarized to the M2 state initially and afterward treated with beta-glucan microparticles. Polarization was tested using the arginase-1 assay and cell supernatant was stored for downstream testing.

Arginase-1 Assay

The arginase assay was performed on cells in 96-well plates as previously established in our lab (Ayaub et al., 2017). Following the cytokine/YBG treatment, the cells were washed twice with ice-cold PBS. Next, cells were lysed in 25 of 0.1% Triton X-100 supplemented with protease inhibitors (200 mM sodium orthovanadate, 0.1 M PMSF, 1 M DTT, and 5 µg/ml and bovine lung aprotinin). A 1:1 dilution with 25 mM of Tris-HCl (pH 7.5) was later performed. 25 µl of this mixture was transferred to a 96-well PCR plate, with the addition of 2.5 µl of 10 mM manganese chloride. The PCR plate was then placed in a thermal cycler programmed to heat at 56 degrees Celsius for 10 minutes. Afterward, 25 µl of 0.5 M L-arginine was mixed with the pre-heated mixture and the entire plate was then incubated at 37 degrees Celsius for 30 minutes. An eight-point urea standard curve was then established (0.625 to 20 mM). 200 µl of acid solution (63.6% water, 9.1% concentrated sulphuric acid and 27.3% concentrated phosphoric acid), followed by 10 µl of 9% alpha-isonitrosopropiophenone, were added to both samples and the urea solutions. The contents of each well were mixed thoroughly, and the plate was incubated at 95 degrees Celsius for 30 minutes, followed by 5 minutes of cooling at 20 degrees Celsius. 150 ul of each sample was removed and placed in a new, clear, flat bottom, 96-well plate for absorbance reading at 550 nm.

LDH Assay

LDH presence in cell supernatant was assessed via the LDH Cytotoxicity Assay Kit (Thermofisher cat# C20301), as an indicator of compound mediated cytotoxicity, manufacturer protocol was followed.

Flow Cytometry

BMDMs (WT and Dectin-1 KO) seeded at 5 million cells per 60 x 15 mm tissue culture plate were treated according to the co-treatment or polarized angles, as described above. After the treatment was ended the adherent macrophages were lifted off the plate using 3 ml of Accutase and placed in a cell staining buffer (0.5% BSA in PBS). Non-antigen-specific binding of immunoglobulins to Fcγ II/ III receptor was blocked using purified rat anti-mouse CD16/32 antibody (Mouse FC Block) (BD Biosciences). Next, the cells were stained for cell surface antibodies anti-mouse CD11b ((BioLegend, Cat#: 101259), and anti-mouse CD206 (MMR) (Biolegend, Cat# 141734). Propidium iodide (PI) was used to assess cellular viability according to the manufacturer's protocol (ThermoFisher Scientific). Lastly, the cells were suspended in a cell staining buffer for flow cytometry and data was collected using a BD LSRFortessa^{TM} LSRII and FACSDiva software (BD Biosciences). Data analysis was performed using the FlowJo software. All staining and flow analyses were performed by Dr. Olivia Mekhael.

THP-1 Derived Macrophage Culture

THP-1 monocytes were propagated in RPMI-1640 media (10% FBS, 1% pen/strep, 1% glutamine). At passage 14 cells were plated in a 96-well plate at a density of 80 000 cells per well and terminally differentiated into macrophages was induced using Phorbol Myristate Acetate (PMA) at 10ng/ml for 48 hours.

To obtain hyperpolarized M2 macrophages an anti-inflammatory cytokine cocktail comprised of human recombinant IL-4 (20 ng/ml; Cedarlane catalog # 200-04-20UG), IL-13 (20 ng/ml; Cedarlane catalog # 200-06-20UG), and IL-6 (5ng/ml; Cedarlane catalog # 200-13-10UG) was used. Treatment time was 72 hours. To obtain M1 macrophages a pro-inflammatory cytokine cocktail of lipopolysaccharide (LPS; 100ng/ml; Sigma catalog # 82857-67-8) and human recombinant interferon-gamma (IFNγ; 10ug/ml; Sigma catalog # MFCD00131391) was used.

Phagocytosis Assay and Fluorescent Imaging

Aniline blue staining of PGX beta-glucan (20F17) was done as described previously (Okada & Ohya, 2016). Briefly, 2 mg of 20F17 was stained with 2 milliliters of a 5 mg/ml solution of aniline blue in PBS (Sigma Cat# 28631-66-5) for 5 min, vortexed, and then centrifuged at 10000 RPM for 1 minute, and then decanted. The microparticles were washed with 2 ml of PBS, pelleted via centrifugation, and then decanted. The microparticles were washed three times in total to discard unbound stain.

BMDMs (wildtype and dectin-1 KO) and THP-1 macrophages, naïve and M2 polarized, were seeded in a black bottom 96-well plate were treated with fluorescent

20F17 microparticles (100 ug/ml or 10 ug/ml). After 1 or 6 hours of treatment, the wells were washed with warm PBS twice. 150 ul of PBS was added to all wells and the 96-well plate was read using fluorescent spectroscopy. The excitation wavelength was adjusted to 395 nm and the emission wavelength was adjusted to 495 nm, as recommended by Wood et al., who describe aniline blue staining of 1-3 linkage yeast beta-glucans (Wood & Fulcher, 1984).

Microparticle location in naive/M2 macrophages was visualized using the EVOS® FL Cell Imaging microscope from Thermo Fisher Scientific at 40X magnification and using the DAPI color filter cube.

Animals and administration of bleomycin and beta-glucan microparticles

11–12 week wild-type female C57BL6/J mice were purchased from Charles River Laboratories and housed in McMaster University's Central Animal Facility. The animals were kept on a 12 h light/12 h dark cycle at a temperature of 20–25 °C, with a humidity of ~50%, and fed *ad libitum*. All work was conducted under the guidelines of the Canadian Council on Animal Care and approved by the Animal Research Ethics Board of McMaster University under Protocol #190823. Experimental pulmonary fibrosis was induced using oropharyngeal intubation of bleomycin at 0.05 U/mouse in a volume of 50 ul sterile saline (0.9% NaCl). Naive control mice were given 50 ul sterile saline. Experimental groups were given 20 ug or 2 ug of 20F17 or 2 ug NTB-YBG in 50 ul sterile saline on day 7 (injury phase) after bleomycin administration. Select groups were

given a second administration of 20 ug or 2 ug of 20F17 or 2 ug NTB-YBG at day 14. All mice were sacrificed 21 days (fibrotic phase) after bleomycin administration.

Mouse sample collection

Mice were anesthetized with a ketamine-xylazine solution (K, 100 mg/kg; X, 10 mg/kg). The trachea was cannulated and the lung was washed with phosphate-buffered saline (1 ml per mouse) for bronchioalveolar lavage fluid (BALF) collection. The mouse abdomen was opened, and blood was collected via the inferior vena cava and placed in a tube coated with EDTA. Whole blood was spun down (1500 RMP, 4 degrees Celsius, 10 mins), with plasma being collected and stored at -80 degrees Celsius for downstream assessment. The four lobes of the right lung were tied up with a surgical thread and excised. The superior lobe was homogenized and stored in TRIzol reagent for downstream RNA extraction, and the remaining lobes were homogenized in 1 ml of PBS and spun down (1500 RMP, 4 degrees Celsius, 10 mins) to collect lung homogenate, with the remaining cell pellet being resuspended in 1 ml of RIPA buffer with added aprotinin protease inhibitor for downstream protein analysis. The left lung was inflated with a 10% formalin solution under a pressure of 30 cmH_2O. The lungs were fixed for 24 hours before submission to the Histology Core facility for paraffin wax embedding and histological analysis. BALF was spun down (14000 RPM, 4 degrees Celsius, 10 minutes), the supernatant was collected and stored at -80 degrees Celsius for later cytokine assessment. BAL cells were resuspended in 1 ml PBS and 150 ul was used for cytospins

and submitted to the Histology Core facility for Wright-Giemsa staining to allow for cell differential analysis.

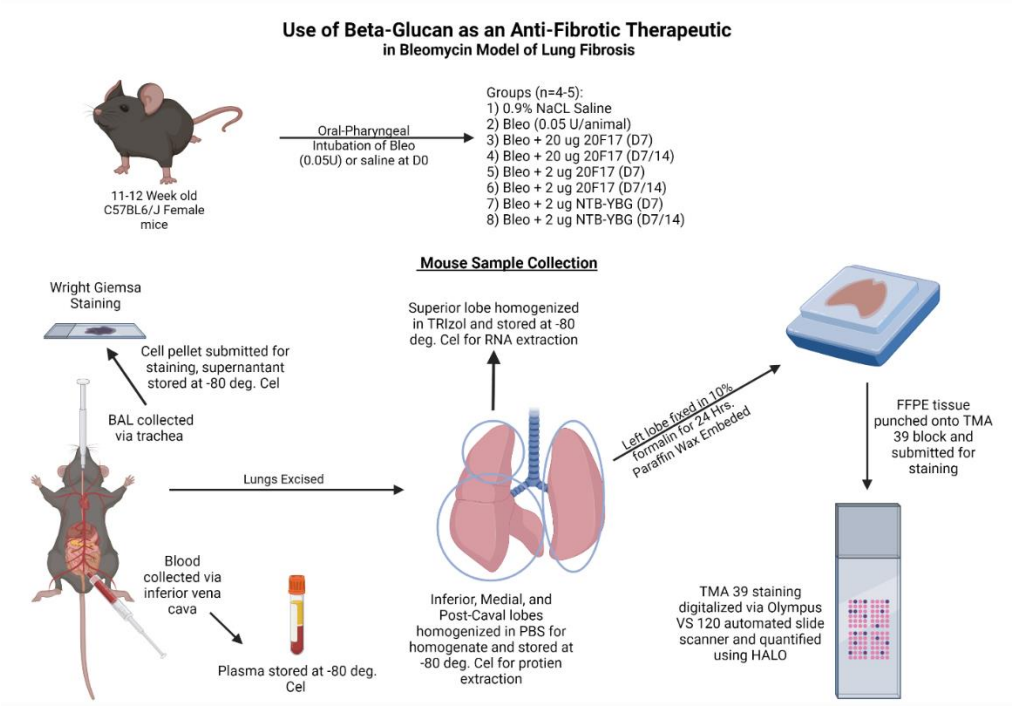

Created with BioRender.com

Figure 5: Overall workflow for animal study and sample acquisition

As depicted above wildtype (C57BL6/J) mice were intubated with either bleomycin (0.05 units per animal) or 0.9% NaCl saline at Day 0. Further intubation with 20F17, saline, or NTB-YBG occurred on Day 7 and 14 for the corresponding groups. The mouse sample collection procedure occurred on Day 21 and samples were accordingly collected.

ELISA

Commercially available ELISA kits were used for mouse sample cytokine measurement for TNFa (Bio-Techne, Cat# DY410-05), IL1B (R&D Systems, Cat# DY401), and TGF-B (R&D Systems, Cat# DY1679) according to the manufacturer's protocol.

Cytokine secretion in THP-1 cell supernatants was measured using a commercially available ELISA kit, according to the manufacturer's protocol for CCL18 (R&D Systems, Cat# DY394), and TNFa (R&D Systems, Cat# DY210).

Sircol Collagen Assay

Lung homogenate, the supernatant following lung homogenization in PBS, was used to assess soluble lung collagen content, according to the manufacturer's instructions (Sircol™ Soluble Collagen Assay, Biocolor, UK).

Total Nitric Oxide Assay

Nitrate measurement in proxy of nitric oxide was made in cell supernatants by the Total Nitric Oxide and Nitrate/Nitrite Parameter Assay Kit according to manufacturer instructions (R&D Systems, Cat# KGE001).

Tissue Microarray Generation

A TMA with mouse left lobe tissues from the animal study (objective 3) was generated by Molecular Phenotyping and Imaging Core (MPIC) facility's technician Amir Reihani, based in St. Joeseph's Hospital Hamilton, Ontario. Regions were randomly selected from Formalin-Fixed Paraffin-Embedded (FFPE) tissue blocks and then punched and inserted into a new paraffin block using the TMA Master II (3D Histech Ltd) for the creation of mouse TMA 39. Each FFPE block was punched twice to obtain two technical replicates per animal on the TMA. For histological sections, paraffin blocks were cut into individual 5µm serial sections and stained.

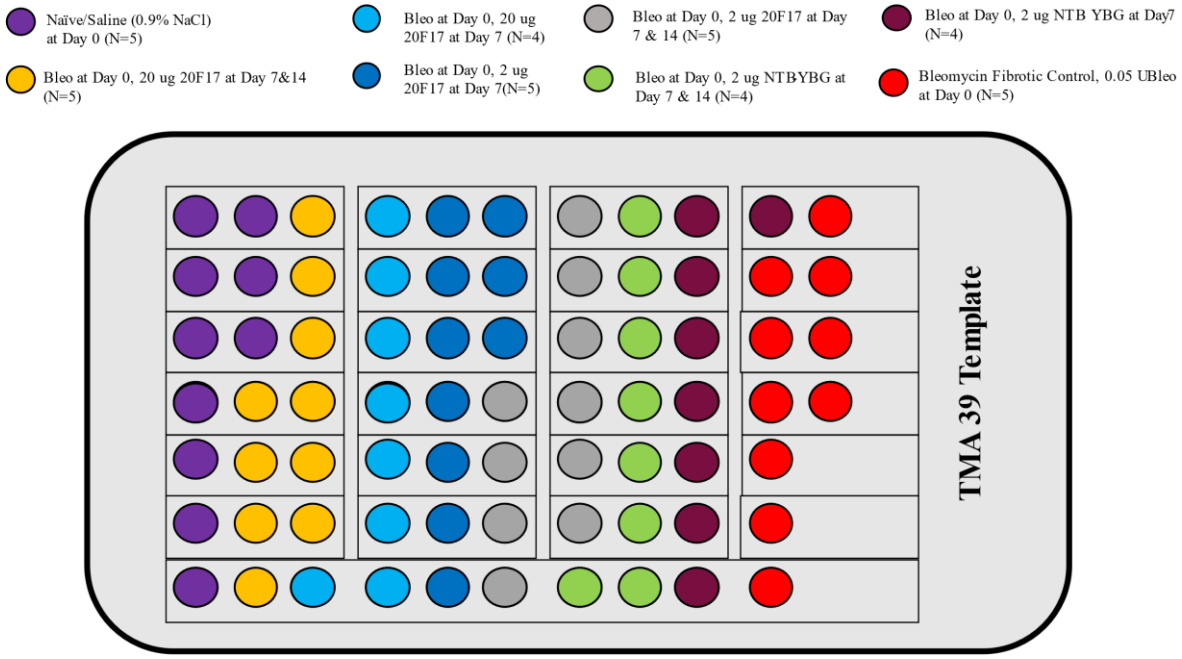

Figure 6: Mouse TMA 39 design

A visual outline of tissue microarray block. The legend above image displays group IDs and biological replicate numbers. Two cores from each biological replicate (randomly selected from the FFPE block) were punched onto the TMA block.

Immunohistochemistry (IHC)

IHC staining was performed by the McMaster Immunology Research Centre's John Mayberry Histology Facility, using the Bond RX immunostainer (Leica).

Image Acquisition

The was used to image slides. IHC and Masson's Trichrome stained slides were imaged at 20x magnification and H/E slides were imaged at 40x magnification by MPIC's Spencer Revill.

HALO Image Quantification

HALO® histological image analysis software (Indica Labs, San Diego CA) was used to measure staining levels in TMA cores. A specific algorithm relative to each stain's color, intensity, and optical density was generated. Percent cell positivity in IHC stains was detected via the Multiplex IHC module. All histology quantification and image creation were done by MPIC's Spencer Revill.

Statistical Analysis

All results were expressed as mean ± standard error of the mean (SEM). All graphs and statistical tests were performed using GraphPad Prism 9.2.0 (GraphPad Software, Inc). Two-way ANOVA followed by Tukey's multiple comparisons test was used to determine significance when more than two groups were compared. A $p < 0.05$ was considered statistically significant.

RESULTS

Objective 1: Assess M2 macrophage polarization in the presence of beta-glucan microparticles

1.1 20F17 inhibits M2 polarization in naive macrophages with no noticeable cytotoxicity

To determine the effect of yeast-derived PGX beta-glucan (20F17) and how it influences the *in vitro* M2 polarization of naïve macrophages, we treated naive macrophages from wild-type mice with our well-established M2 polarization cocktail (IL-4, IL-13 & IL-6) and varying concentrations of 20F17 concurrently. We used arginase-1 activity, measured as mM of urea, as a marker for M2 polarization. The M2 phenotype has a robust increase in arginase-1 relative to M0 (naïve) and M1 (pro-inflammatory) macrophages, especially when IL-6 is part of the polarization cocktail (Ayaub et al., 2017). Figure 7 A) shows a significant increase ($p<0.0001$) in arginase-1 activity in the M2 group (positive control) relative to the M0 group (negative control). There is a noticeable decrease seen in the arginase-1 activity in treatment groups starting at the concentration of 10 ug/ml and further reduced at 100 ug/ml. The decrease seen in arginase-1 activity is dose-dependent with maximal inhibition occurring at 100 ug/ml and an insignificant decrease, relative to the 100 ug/ml concentration, occurring at 1000 ug /ml. To verify that the change in activity is not due to 20F17 mediated cytotoxicity, Figure 7 B) shows LDH release as a percentage in treatment groups relative to lysed cells. Even at a very high 20F17 concentration of 1000 ug/ml, there is no significant difference seen in LDH release.

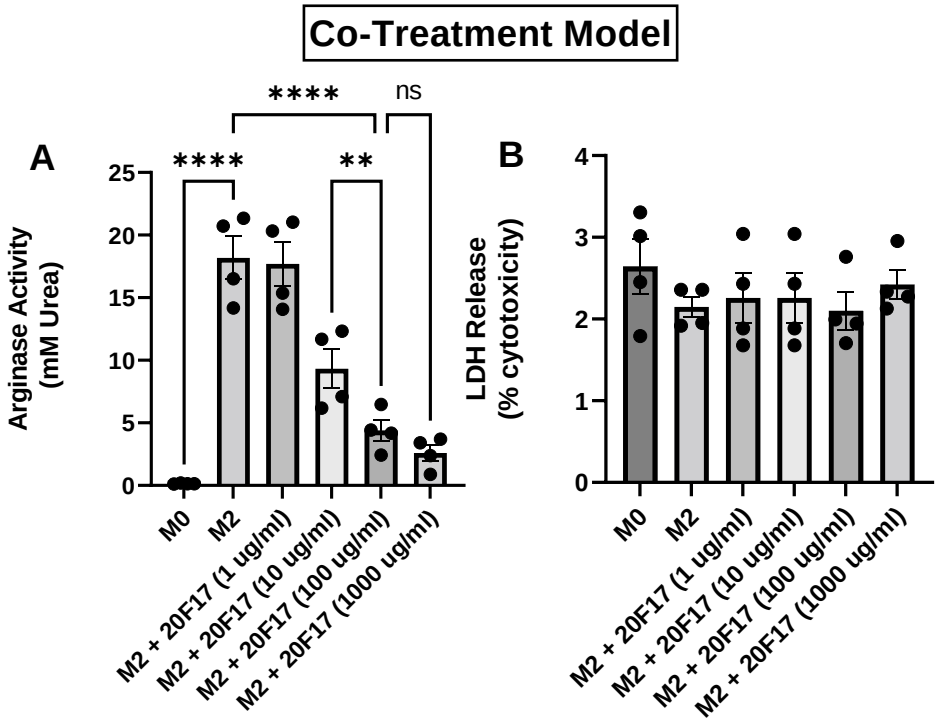

Figure 7: Examining arginase-1 activity in naive macrophages treated with M2 cocktail and 20F17

Beta-glucan (20F17) intervention in a co-treatment M2 polarization assay with WT BMDMs yields differences in arginase-1 activity relative to beta-glucan concentration at 24 hours of treatment. 20F17 and IL-4/IL-13/IL-6 co-treatment show significant inhibition of arginase-1 production starting at the 10 ug/ml concentration (A), with no significant changes in LDH release caused by varying concentrations of 20F17 (B). Bar graphs represent mean ± SEM from 4 biological replicates per group, $^{**}p < 0.01$; $^{****}p < 0.0001$, n = 4. Significance was established using GraphPad, Prism 9.0 with Two-way ANOVA using Tukey's Multiple Comparison Test.

1.2 Yeast-derived PGX beta-glucan (20F17) inhibits M2 polarization at the 100 ug/ml concentration at the same degree as non-PGX yeast beta-glucan (YBG)

An essential part of this objective is to assess how a variety of different beta-glucan types with different glycosidic linkages, as mentioned in Table 1, affect the M2 polarization of naïve macrophages. As such, we set up a co-treatment polarization assay to test how well non-PGX yeast beta-glucan (YBG), oat beta-glucan (OBG), nintedanib

impregnated beta-glucan (NTB-YBG), and Zymosan (Zymo) compare to 20F17's ability to inhibit M2 polarization in wildtype naïve macrophages. We used a concentration of 100 ug/ml since maximal inhibition occurs there, as is suggested by Figure 7 A). Another goal here was to see if our key PGX yeast beta-glucan microparticle (20F17) was different in inhibiting M2 polarization when compared to the non-PGX yeast beta-glucan (YBG) microparticle. Figure 8 shows that 20F17, YBG, NTB-YBG, and Zymosan all inhibit arginase-1 activity at the 100 ug/ml concentration to the same degree ($p<0.0001$) relative to the M2 control group, however, 20F17 does this with the least variability. There is no significant difference between 20F17 and YBG's ability to inhibit arginase-1 activity. OBG does not inhibit arginase-1 activity to the same level as the other microparticles.

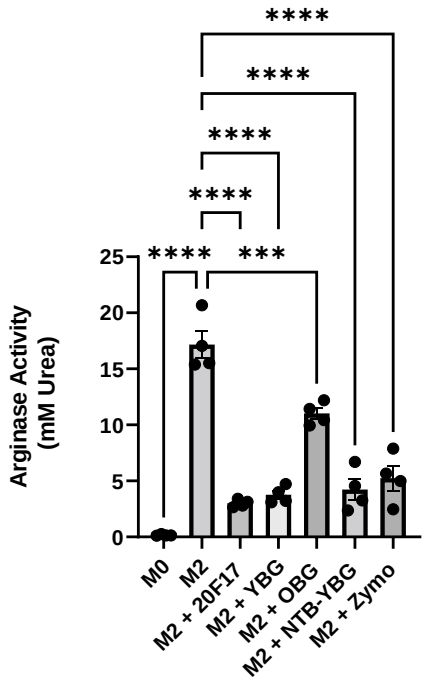

Figure 8: Assessing a variety of beta-glucan types in a compound screen to determine M2 inhibition efficacy at the 100 ug/ml concentration

Beta-glucan screen in a co-treatment M2 polarization assay with WT BMDMs yields differences in arginase-1 activity relative to beta-glucan variety at 24 hours of treatment. All beta-glucan varieties inhibit arginase-1 activity relative to the M2 group at the 100 ug/ml concentration, with OBG not causing as significant a decrease as the other varieties. Arginase-1 activity is similar between 20F17 (PGX yeast beta-glucan) and YBG (non-PGX yeast beta-glucan) treated groups. Bar graphs represent mean ± SEM from 4 biological replicates per group, ***$p < 0.001$; ****$p < 0.0001$, $n = 4$. Significance was established using GraphPad, Prism 9.0 with Two-way ANOVA using Tukey's Multiple Comparison Test.

1.3 20F17 inhibits arginase-1 activity and frequency of CD206 expression in wildtype and dectin-1 knock-out macrophages in the co-treatment model

While arginase-1 is a characteristic enzyme produced by M2 macrophages and is a suitable indicator of alternative activation, we also wanted to study the expression of cell surface marker CD206 which is upregulated by IL4/IL13 (Orecchioni et al., 2019). To carry out this objective a simple flow cytometry panel with staining for CD206 as the M2

marker, and CD11b as the general macrophage marker was designed. CD11b can reliably be used as a macrophage marker for adherent BMDMs (Zajd et al., 2020). Figure 9 shows the gating strategy applied to determine the frequency of CD206+CD11b+ cells in treatment groups. Figure 10 A) shows the arginase-1 inhibition caused by 20F17 in naïve wildtype (WT) and dectin-1 knockout (KO) macrophages in a dose-dependent manner. Both WT and KO macrophages in the M2 control group show a robust arginase-1 activity meaning that the dectin-1 receptor does not alter the propensity of arginase-1 expression. 20F17, at 10 and 100 ug/ml, causes a more significant decrease in arginase-1 expression in WT macrophages relative to KO macrophages. The frequency of CD206 expression is upregulated in the M2 positive control group for both WT and KO macrophages relative to the M0 negative control group (B). The frequency of CD206 expression is significantly higher in the WT-M2 group in comparison to the KO-M2 group ($p<0.001$). The decrease in CD206 expression due to 20F17 is dose-dependent as only the 100 ug/ml concentration shows lowered CD206+ cells. In line with figure 7 B) There are no significant changes in the frequency of live cells in the wildtype macrophages, however the KO group treated with 100 ug/ml 20F17 has a significantly decreased frequency of live cells (C).

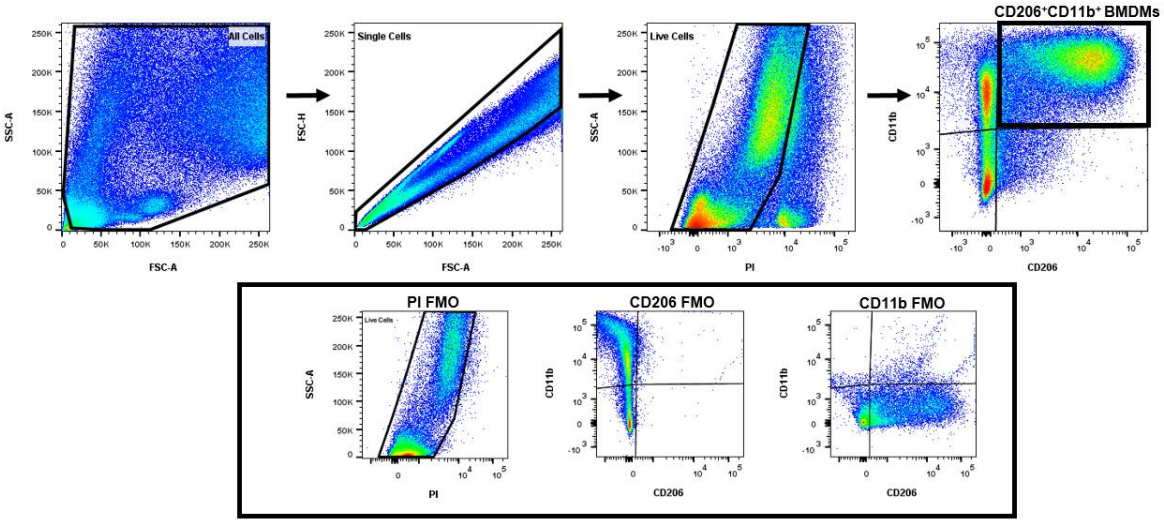

Figure 9: Flow cytometry gating strategy utilized to identify M2-polarized macrophages ex vivo

Single cells were gated from all cells to exclude doublets and debris, then total PI- live cells were isolated. CD206+CD11b+ M2-polarized macrophages were gated from total live cells. Fluorescence minus one (FMO) was used to gate the cells.

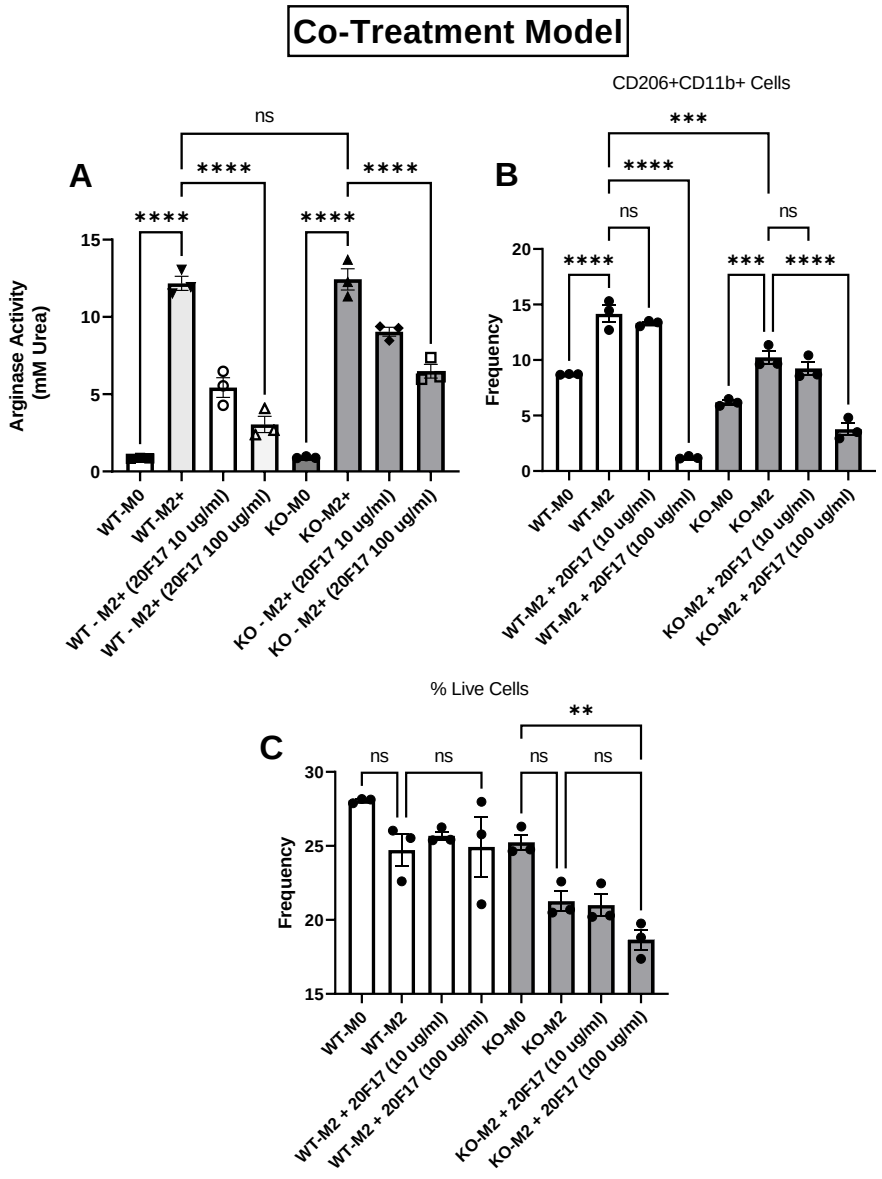

Figure 10: 20F17 inhibits arginase-1 activity and frequency of CD206+ expression in wildtype and dectin-1 -/- (KO) macrophages co-treated with IL4/IL13/IL16

20F17 intervention in a co-treatment M2 polarization assay with wildtype (WT) and dectin-1 -/- (KO) BMDMs yields inhibition in arginase-1 activity and frequency of CD206 expression in a dose-dependent manner at 24 hours. 20F17 and IL-4/IL-13/IL-6 co-treatment show significant inhibition of arginase-1 production at the 100 ug/ml concentration for both WT and KO macrophages (A-B). There are no significant changes in the frequency of live cells in the wildtype macrophages, the KO group treated with 100 ug/ml 20F17 has a significantly decreased frequency of live cells (C). Bar graphs represent mean ± SEM from 3 biological replicates per group, $^{**}p < 0.01$; $^{***}p<0.001$; $^{****}p < 0.0001$, n = 3. Significance was established using GraphPad, Prism 9.0 with Two-way ANOVA using Tukey's Multiple Comparison Test.

1.4 M2 polarized macrophages (treated with 20F17 do not show decreases in arginase-1 activity

20F17 inhibits arginase activity in naïve macrophages with the co-treatment model, however, we also wanted to assess how arginase activity changes in polarized M2 macrophages. Naive (M0) macrophages were polarized to the M2 state by treating with an IL4/IL13/IL6 cytokine cocktail for 24 hours. After 24 hours the cytokine treatment was removed and substituted with a 1-1000 ug/ml 20F17 treatment (except for M0 and M2 groups that received a media change) for an additional 24 hours. To assess 20F17 mediated cytotoxicity, Figure 11 B) shows LDH release as a percentage in treatment groups relative to lysed cells. Even at a very high 20F17 concentration of 1000 ug/ml, there is no significant difference seen in LDH release.

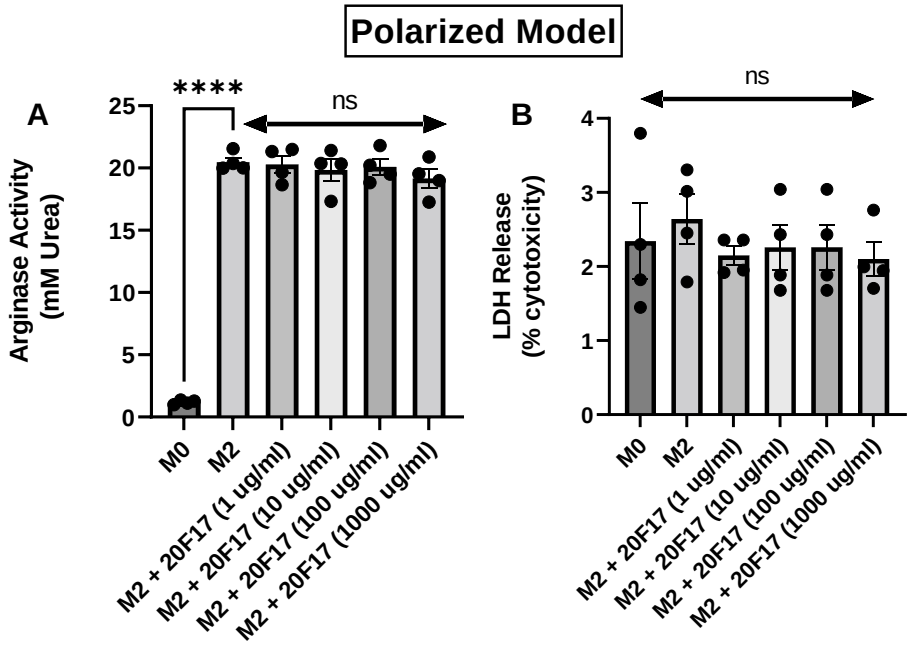

Figure 11: Polarized M2 macrophages (24 hours IL-4/IL-13/IL-6) treated with 20F17 (1 ug to 1000 ug /ml) do not show decreases in arginase-1 activity

Arginase-1 activity is significantly increased in M2 treated wildtype BMDMs relative to naïve (M0) control and is not significantly different in the 20F17 treatment groups (A). % cytotoxicity based on LDH release is not significantly different among control and 20F17 treated groups. Bar graphs represent mean ± SEM from 4 biological replicates per group, ****$p < 0.0001$, $n = 4$. Significance was established using GraphPad, Prism 9.0 with Two-way ANOVA using Tukey's Multiple Comparison Test.

1.5 20F17 decreases frequency of CD206 expression in wildtype and dectin-1 knock-out macrophages in the polarized model

To determine how the expression of cell surface receptor CD206 changes in polarized M2 macrophages after a 20F17 intervention we used the flow panel and gating strategy as described above (Figure 9) to assess treatment groups. Figure 12 A) shows that while both WT and KO M2 treatment groups show a comparable and robust increase in arginase-1 activity relative to the M0 controls, 20F17 at the 100 ug/ml concentration does not change arginase-1 activity. This provides further support to the data presented in Figure 11 A). Figure 12 B) shows that the frequency of CD206 expression in M2 macrophages treated with 100 ug/ml of 20F17 is lowered relative to the M2 control in both WT and KO groups. While CD206 expression in WT and KO M2 treated with 20F17 is not significantly different, the variability is a lot less in the WT macrophages. There are no significant changes in the frequency of live cells in the KO macrophages, the WT group treated with 100 ug/ml 20F17 has a significantly higher frequency of live cells relative to the WT-M2 group, suggesting that perhaps 20F17 might be beneficial for M2 viability in WT macrophages(C).

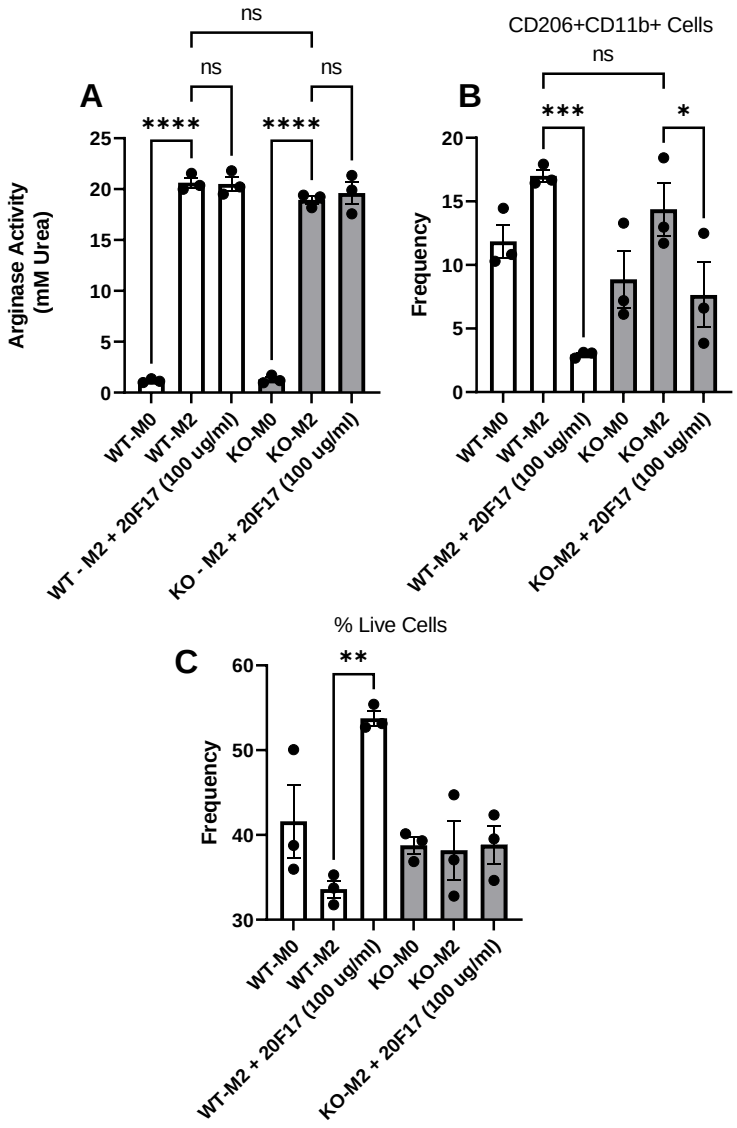

Figure 12: 20F17 inhibits frequency of CD206+ expression in wildtype and dectin-1 -/- (KO) in polarized M2 macrophages

20F17 intervention in an M2 polarized wildtype (WT) and dectin-1 -/- (KO) BMDMs shows no change in arginase-1 activity but decreases the frequency of CD206 expression after 24 hours of treatment (A-B). There are no significant changes in the frequency of live cells in the KO macrophages, the WT group treated with 100 ug/ml 20F17 has a significantly higher frequency of live cells relative to the WT-M2 group(C). Bar graphs represent mean ± SEM from 3 biological replicates per group, **$p < 0.01$; ***$p<0.001$; ****$p < 0.0001$, $n = 3$. Significance was established using GraphPad, Prism 9.0 with Two-way ANOVA using Tukey's Multiple Comparison Test.

1.6 20F17 triggers polarized alternatively activated "M2" macrophages to exhibit classically activated "M1" characteristics

Lie et al., have shown that immunosuppressive TAMs display a dectin-1 dependent upregulation of M1 genes post a 100 ug/ml whole glucan particle intervention (2015). We wanted to explore whether there are dectin-1 dependent M1-like functional changes occurring in polarized M2 macrophages post 20F17 treatment. The M1 phenotype is induced using LPS and INF-y and these macrophages produce abundant pro-inflammatory cytokines like TNF-a, as well as NO (nitric oxide) from upregulation of iNOS(Murray & Wynn, 2011; Orecchioni et al., 2019). NO is readily broken down into nitrite and nitrate. To assess M1 markers in our 20F17 treated polarized M2 macrophages we utilized a TNF-a ELISA and a nitrite test (in proxy of NO measurement). Figure 13 A/C shows that WT and KO BMDMs polarized to the M1 state are strong producers of TNF-a and nitrite. WT-M1 and KO-M1 production of nitrite are not significantly different, however, KO-M1 macrophages produce a significantly higher amount of TNFa ($p<0.003$). TNF-a and nitrite production in M1 polarized WT and KO macrophages is not significantly changed after a 100 ug/ml 20F17 treatment. Nitrite production is significantly increased in WT-M2 macrophages treated with 20F17 in a dose-dependent manner relative to WT-M2 control, with 100 ug/ml producing significantly more than 10 ug/ml (B). This trend is absent in KO macrophages, suggesting NO production to be dectin-1 dependent. TNF-a release increases in M2 macrophages treated with 20F17, however, the increase is more pronounced in the WT. WT-M2 treated with 100 ug/ml 20F17 produces significantly higher levels of TNF-a than KO-M2 ($p<0.0001$).

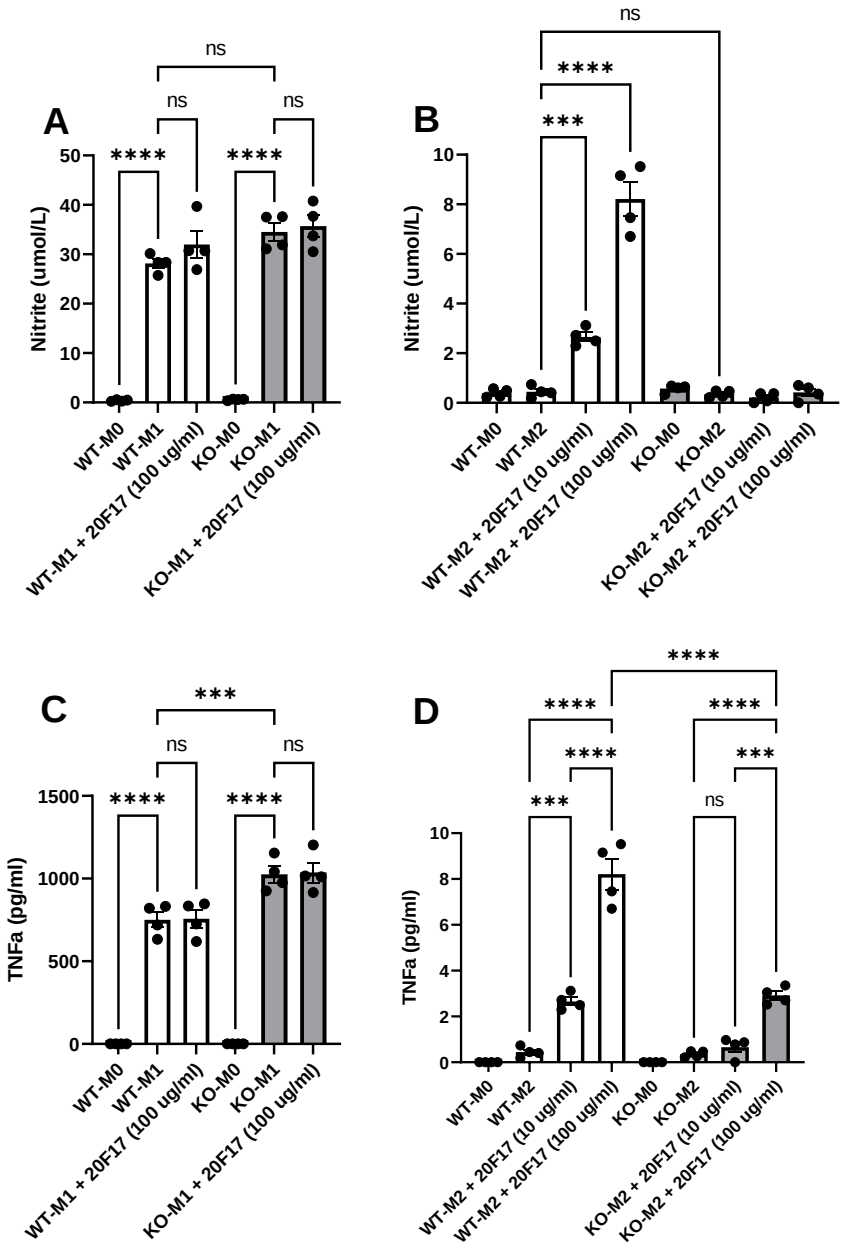

Figure 13: Polarized M2 macrophages produce TNF-a and nitrite in a dectin-1 dependent manner post 20F17 treatment

20F17 intervention in an M2 polarized wildtype (WT) macrophages causes increased production of TNF-a and nitrite after 24 hours of treatment (B/D). There are no significant changes in nitrite production by KO-

M2 macrophages (B). WT and KO M1 macrophages produce significantly higher TNFa and nitrite relative to M0 controls, with M1 treated with 20F17 showing no further changes relative to M1 (A/C). Bar graphs represent mean ± SEM from 4 biological replicates per group, ***p<0.001; ****p < 0.0001 , n = 4. Significance was established using GraphPad, Prism 9.0 with Two-way ANOVA using Tukey's Multiple Comparison Test.

1.7 20F17 co-treatment partly inhibits CCl18 production in M2 macrophages

To assess how well 20F17 works in a human macrophage model we used monocyte-derived THP-1 macrophages. Monocytes were treated with PMA for 48 hours and resulting terminally differentiated M0 macrophages were co-treated with IL4/IL13/IL6 and varying concentrations of 20F17 for 24 hours. Relevant to THP-1 macrophages, CCL18 is a well-characterized marker for M2 polarization that has clinical importance as well (Ask et al., 2017). CCl18 expression by M2-like macrophages is directly involved in initiating collagen production by fibroblasts and furthers fibrogenesis (Prasse et al., 2006). Figure 14 shows that CCL18 production in M2 macrophages is significantly higher than in the M0 negative control. 20F17 treatment causes a significant (p,0.01) but rather a small decrease in CCl18 production at the 1000 ug/ml concentration, smaller concentrations causing no significant changes in CCL18 relative to the positive M2 control.

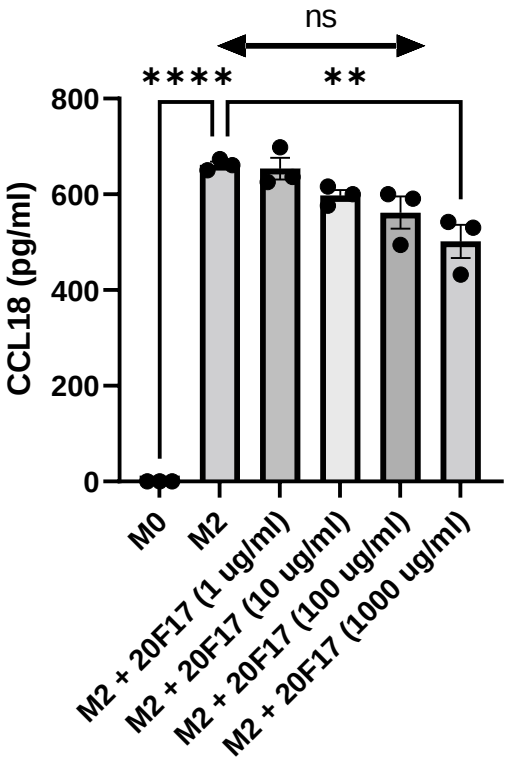

Figure 14: CCL18 release in THP-1 macrophages co-treated with 20F17 and IL4/IL13/IL6

CCL18 release in THP-1 monocyte-derived macrophages co-treated with 20F17 and human M2 cytokines (IL-4, Il-13, Il-6) for 24 hours. Only 1000 ug/ml of 20F17 significantly lowered CCL18 production relative to M2+ control macrophages. Bar graphs represent mean ± SEM from 3 technical replicates per group,****$P < 0.0001$, n = 3. Significance was established using GraphPad, Prism 9.0 with Two-way ANOVA using Tukey's Multiple Comparison Test.

1.8 1000 ug/ml 20F17 treatment on M2 polarized THP-1 macrophages initiates TNF-a production

To see if 20F17 causes a difference in M2 polarized THP-1 macrophages we polarized naïve THP-1 macrophages with IL4/IL13/IL6 for 24 hours and subsequently treated with 1-1000 ug/ml of 20F17. TNF-a release assessment was also done to see if 20F17 causes M2 polarized THP-1 macrophages to exhibit M1-like characteristics.

Figure 15 A) shows that while CCL18 production in the M2 groups is significantly higher relative to the M0, 20F17 does not significantly change CCL18 production in polarized M2 THP-1 macrophages. M1 THP-1 macrophages treated with LPS and INF-y produce a significantly higher amount of TNF-a relative to M0 ($p<0.0001$), while 20F17 treatment on M1 does not significantly change TNF-a production (B). M2 polarized THP-1 macrophages produce significantly higher levels of TNF-a relative to M2 control, post a 1000 ug/ml 20F17 treatment (C).

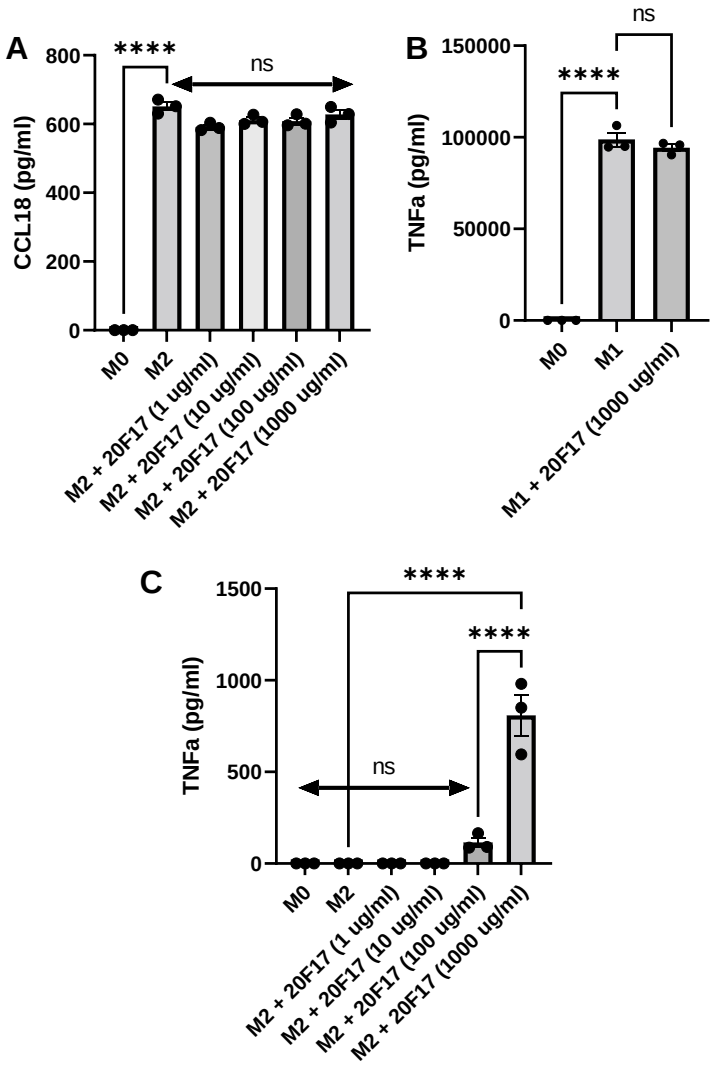

Figure 15: M2 Polarized THP-1 macrophages treated with 20F17 (1 to 1000 ug /ml) do not show changes in CCL18 synthesis

CCL18 release in M2 polarized THP-1 monocyte-derived macrophages treated with 20F17. No significant changes in CCL18 production post 24 hours of 20F17 treatment(A). M1 polarized THP-1s produce significantly higher levels of TNF-a (B). M2 polarized THP-1s produce TNF-a when treated with 1000 ug/ml 20F17. Bar graphs represent mean ± SEM from 3 technical replicates per group, ****$P < 0.0001$, n = 3. Significance was established using GraphPad, Prism 9.0 with Two-way ANOVA using Tukey's Multiple Comparison Test.

Objective 2: Examine uptake of labeled microparticles by macrophages in a phagocytosis assay

2.1 Fluorescent tagging of 20F17 with aniline blue

To perform phagocytosis/uptake studies we had to synthesize fluorescently tagged 20F17 particles where the dye could be easily visualized and provide a robust signal. Using aniline blue we tagged 20F17 microparticles and visualized them under a fluorescent microscope. Using the EVOS imaging microscope, the particles were imaged with transmitted light and using the DAPI color cube (aniline blue fluoresces in DAPI like settings). The resulting images were overlayed to visualize the aniline blue stain. Figure 16 shows a representative image of the unstained and aniline-blue stained 20F17 microparticles.

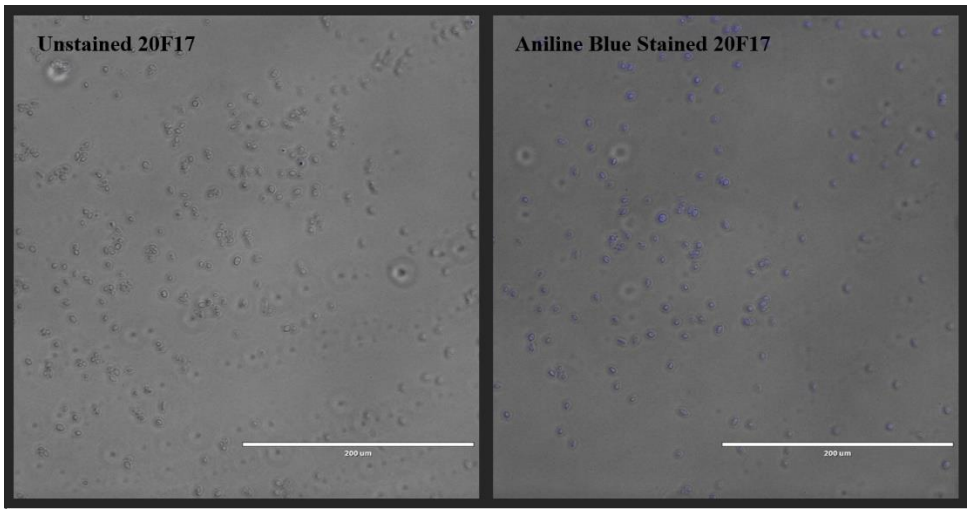

Figure 16: Aniline-blue stained 20F17 microparticles

20F17 microparticles (2 mg) were stained using aniline blue dye and washed with PBS to remove excess dye. Unstained and stained 20F17 samples were suspended in PBS at a concentration of 1000 ug/ml and imaged using the EVOS fluorescent imaging platform.

2.2 Wildtype M2 polarized macrophages show significantly higher uptake of 20F17 at 6 hours

To assess cell-specific uptake of 20F17 microparticles, phagocytosis experiments in WT/dectin-1 KO BMDMs, as well as THP-1 macrophages, were organized. BMDMs from 4 WT and 4 KO mice were isolated and pooled to ensure equal plating density. Macrophages were seeded unto black bottom 96-well plates (80k cells per well), a subset getting M2 polarized. Macrophages were treated with either 100 ug/ml or 10 ug/ml of aniline blue labeled 20F17, with corresponding no-treatment (auto-fluorescence control) and maximal uptake (positive control to determine 100% uptake) groups. Macrophage uptake was assessed at 1 and 6 hours post-treatment using a fluorescent plate reader with the excitation wavelength was adjusted to 395 nm and the emission wavelength was adjusted to 495 nm. M0 and M2 macrophages were treated with 10 or 100 ug/ml 20F17 and assessed for uptake at 1 and 6 hours. There were no significant differences with 20F17 uptake within WT and KO macrophages at 1 hour (A). Uptake is dose-dependent in WT as 100 ug/ml groups display higher uptake relative to 10 ug/ml groups WT-M2 group treated with 100 ug/ml 20F17 had the highest uptake at 6 hours, significantly higher than the KO-M2 group treated with 100 ug/ml 20F17 (B). THP-1 macrophages show no uptake 1-hour post-treatment and only 100 ug/ml treated M0 and M2 show uptake 6 hours post-treatment (C). Figure 18 offers support for the same as the staining in the M2 macrophages is more prominent than the M0 macrophages and staining in WT-M2 treated with 100 ug/ml of labeled 20F17 is highest. Most of the staining on

macrophages appears to be on the cell surface, however, WT-M2 macrophages show a lot of internalized stain, suggesting a greater degree of phagocytosis relative to other groups.

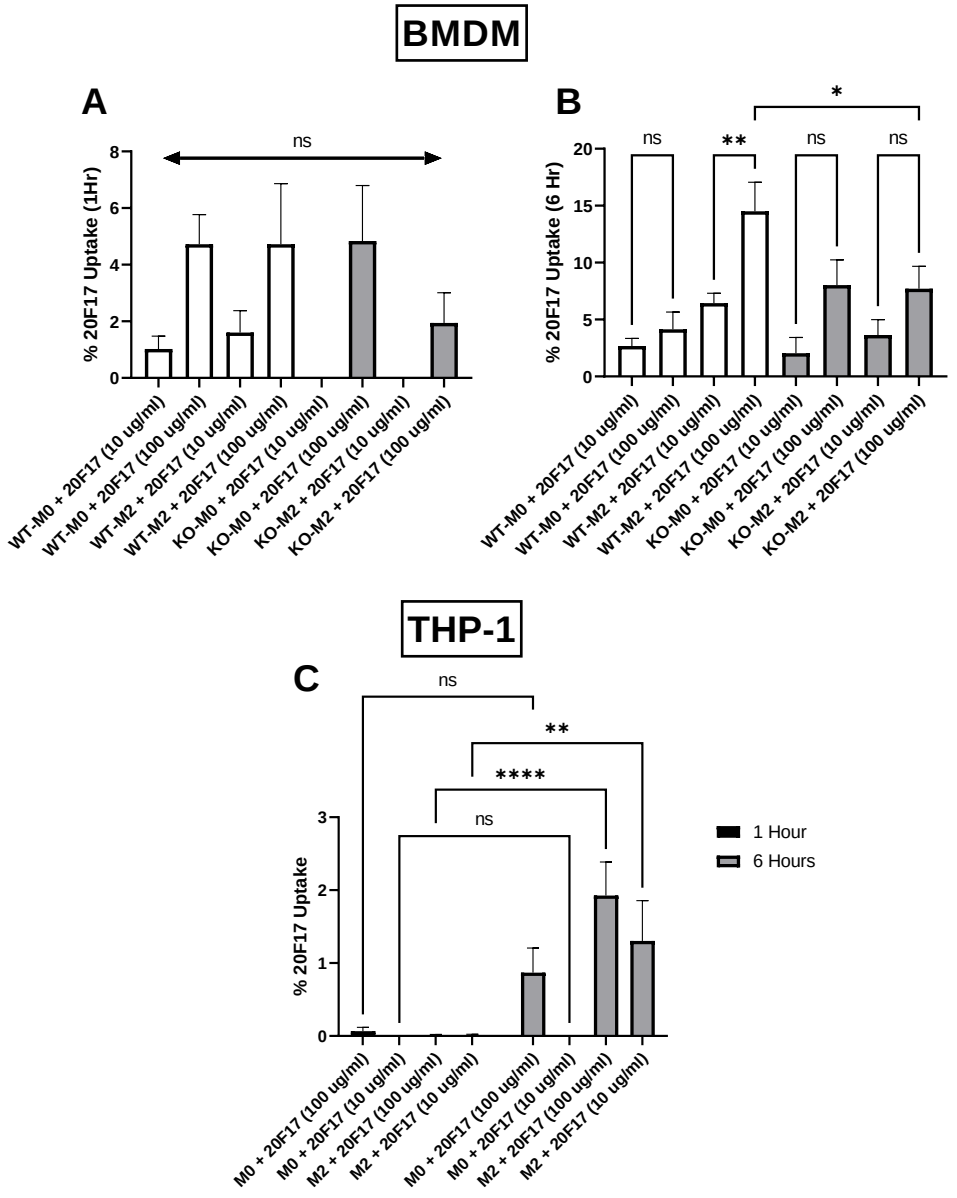

Figure 17: % uptake of aniline blue labeled 20F17 in wildtype (WT) and dectin-1 knockout (KO) BMDMs, as well as THP-1 macrophages

M0 and M2 macrophages were treated with 10 or 100 ug/ml 20F17 and assessed for uptake at 1 and 6 hours. There were no significant differences with 20F17 uptake within WT and KO macrophages at 1 hour (A). Uptake is dose-dependent in WT as 100 ug/ml groups display higher uptake relative to 10 ug/ml

groups WT-M2 group treated with 100 ug/ml 20F17 had the highest uptake at 6 hours, significantly higher than the KO-M2 group treated with 100 ug/ml 20F17 (B). THP-1 macrophages show no uptake 1-hour post-treatment and only 100 ug/ml treated M0 and M2 show uptake 6 hours post-treatment (C). Bar graphs represent mean ± SEM from 6 technical replicates per group, **p<0.01;***p<0.001;****P < 0.0001, n = 6. Significance was established using GraphPad, Prism 9.0 with Two-way ANOVA using Tukey's Multiple Comparison Test.

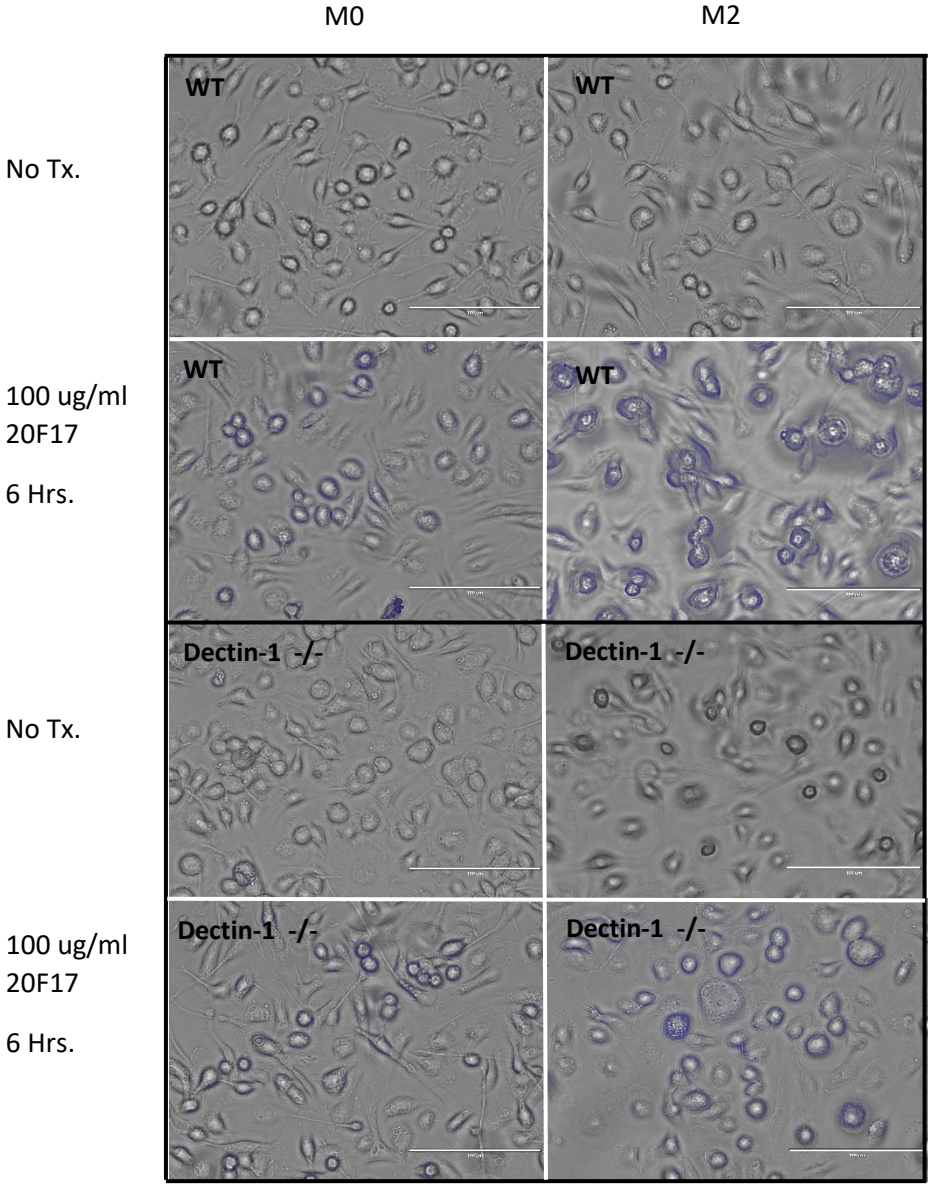

Figure 18: 20F17 uptake in WT and KO (dectin-1 -/-) macrophages

Visualized 20F17 uptake in WT/KO macrophages at 6 hours post-treatment. Cells were imaged in transmitted light and with a DAPI color filter, both images were overlayed to show staining. Staining in the M2 macrophages is more prominent than the M0 macrophages. M0/M2 cells without treatment were shown

as the negative control, there is no discernable auto-fluorescence from untreated cells on the DAPI filter. Images were visualized using the EVOS fluorescent imaging system.

Objective 3: Evaluate the use of 20F17/NTB-YBG microparticles as anti-fibrotic therapeutics in the bleomycin model of fibrotic lung disease

3.1 Beta-glucan intervention in the mouse model of bleomycin shows high survival and decreased soluble collagen content in lung homogenate

The *in-vivo* design as mentioned in objective 3 was executed giving us information about the role of 20F17 and NBG-YBG and how they work in the bleomycin model of fibrotic lung disease. Referring to the effect of bleomycin on body weight, we saw that 0.05 units of bleomycin cause a loss of 9-11 % weight by day 7 (Figure 19 A). Accordingly, naïve mice given saline did not lose weight. Microparticle intubations started on day 7 with doses of 20 ug to 2 ug of 20F17 and 2 ug NTB-YBG, this treatment was well tolerated and only one mouse reached endpoint (more than 15% weight loss) and had to be sacrificed on Day 17 (part of the Bleo+20 ug 20F17 Day 7 group). Regarding soluble collagen content in the lung, all groups treated with microparticles had significantly lower collagen amounts in their total lung homogenate relative to the bleomycin control group ($p<0.001$)(Figure 19 B). The collagen content in the saline negative control group relative to the positive control bleomycin group was significantly lower ($p<0.0001$).

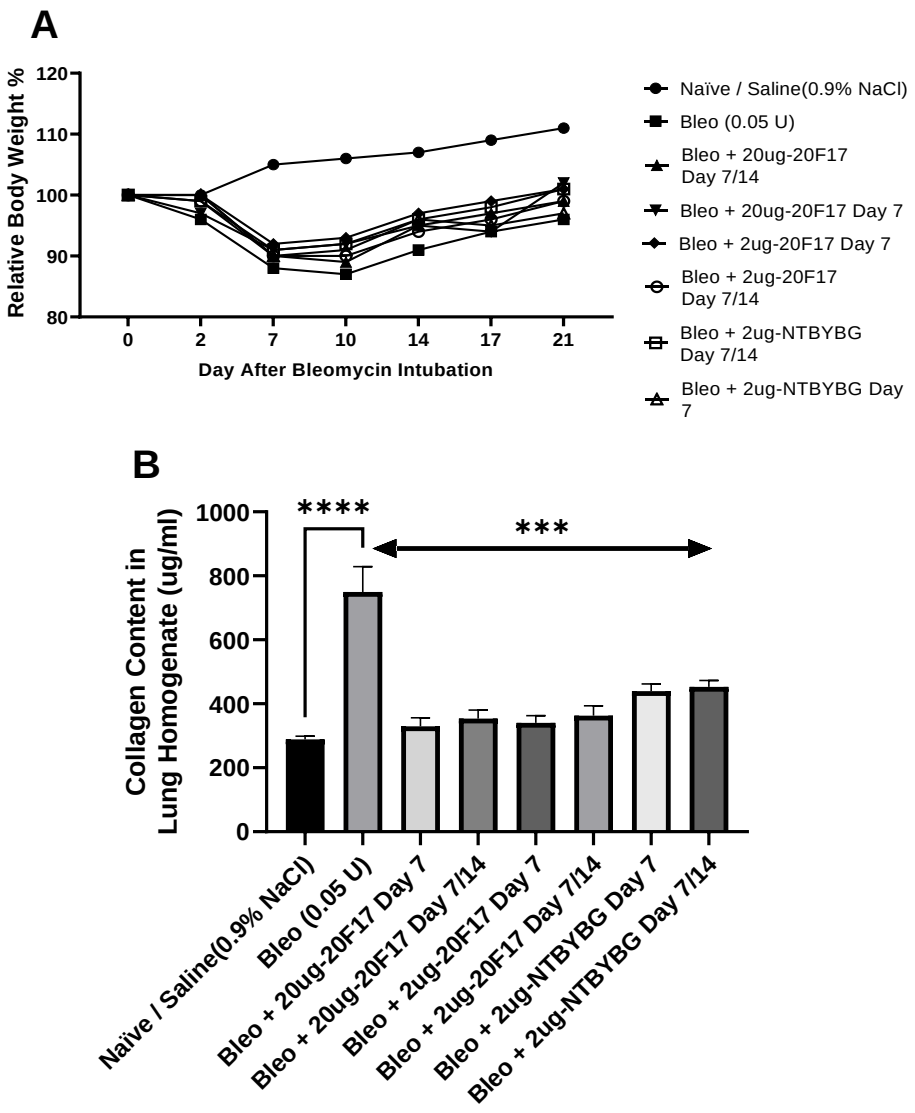

Figure 19: Relative body weight changes and collagen content in lung homogenate of mice given bleomycin and beta-glucan microparticles

Oral pharyngeal intubation of bleomycin (0.05 U/animal) causes a decrease in body weight relative to starting weight and increased soluble collagen content in the lung. Approximately, a 10% decrease in weight is seen in mice given bleomycin 7 days post-intubation (A), relative to saline/vehicle control. Soluble collagen content as measured in lung homogenate from right lobes of treatment mice is significantly lower in 20F17 and NTB-YBG groups relative to the bleomycin control group (B). Bar graphs represent mean ± SEM from 4-5 biological replicates per group, *$P < 0.05$, ****$P < 0.0001$. Significance was established using GraphPad, Prism 9.0 with Two-way ANOVA using Tukey's Multiple Comparison Test.

3.2 20F17 intervention in bleomycin model lowers TNF-a and TFGB in lung homogenate

To assess the immune environment in the lung ELISAs for TGFB, TNF-a, and IL-1B to determine if there was a difference in pro-inflammatory vs anti-inflammatory cytokine release. Figure 20 shows total cytokine levels in lung homogenate and bronchoalveolar lavage (BAL) supernatant. There is a marked increase in TNF-a in the lung homogenate of the Bleo group relative to the saline group, with all 20F17 groups decreasing TNF-a significantly relative to Bleo ($p<0.01$) (A). NTB-YBG groups are not significantly different from TNF-a in lung homogenate when compared to the Bleo group. TNF-a levels in BAL seem to not be significant in all groups except for the 2ug-20F17 day 7 group that shows significantly decreased levels relative to the saline group (D). There is a lot of variability amongst the groups, but the saline group seems to have the highest TNF-a release in the BAL. TGFB in the lung homogenate is significantly higher in the Bleo group, with 20F17 treatments decreasing the release and NTB-YBG failing to do so (B). There are no significant trends in TGFB expression in BAL (E). IL-1B in lung homogenate is again elevated in the Bleo group relative to the saline group but the treatment groups are not significantly different (C). IL-1B in BAL is the highest for the 20ug-20F17 day 7/14 group, all other groups are not significantly different from each other (F).

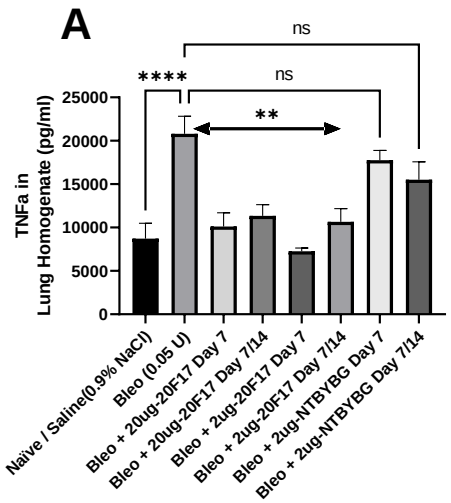
A
TNFa in Lung Homogenate (pg/ml)
25000
20000
15000
10000
5000
0
****
**
ns
ns
Naïve / Saline(0.9% NaCl)
Bleo (0.05 U)
Bleo + 20ug-20F17 Day 7
Bleo + 20ug-20F17 Day 7/14
Bleo + 2ug-20F17 Day 7
Bleo + 2ug-20F17 Day 7/14
Bleo + 2ug-NTBYBG Day 7
Bleo + 2ug-NTBYBG Day 7/14

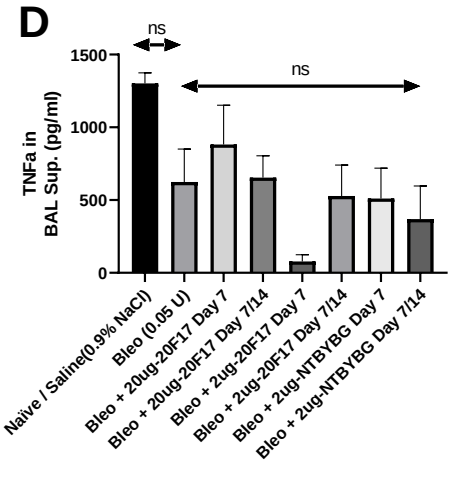
D
TNFa in BAL Sup. (pg/ml)
1500
1000
500
0
ns
ns
Naïve / Saline(0.9% NaCl)
Bleo (0.05 U)
Bleo + 20ug-20F17 Day 7
Bleo + 20ug-20F17 Day 7/14
Bleo + 2ug-20F17 Day 7
Bleo + 2ug-20F17 Day 7/14
Bleo + 2ug-NTBYBG Day 7
Bleo + 2ug-NTBYBG Day 7/14

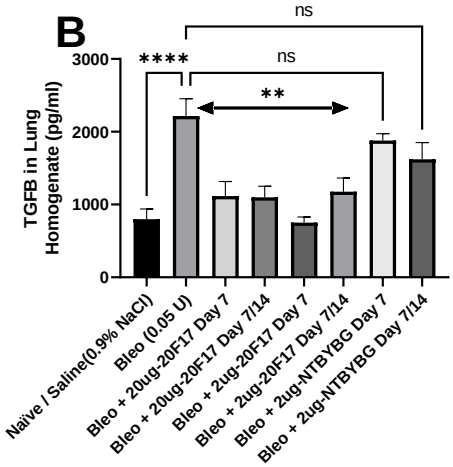
B
TGFB in Lung Homogenate (pg/ml)
3000
2000
1000
0
****
**
ns
ns
Naïve / Saline(0.9% NaCl)
Bleo (0.05 U)
Bleo + 20ug-20F17 Day 7
Bleo + 20ug-20F17 Day 7/14
Bleo + 2ug-20F17 Day 7
Bleo + 2ug-20F17 Day 7/14
Bleo + 2ug-NTBYBG Day 7
Bleo + 2ug-NTBYBG Day 7/14

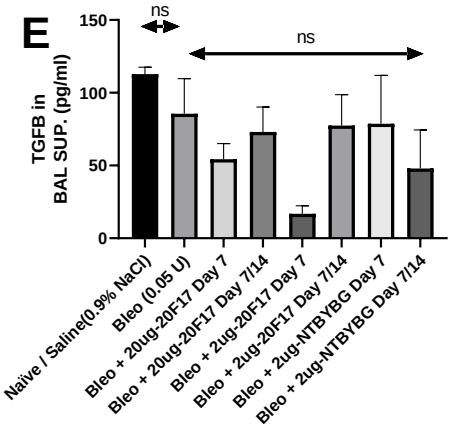
E
TGFB in BAL SUP. (pg/ml)
150
100
50
0
ns
ns
Naïve / Saline(0.9% NaCl)
Bleo (0.05 U)
Bleo + 20ug-20F17 Day 7
Bleo + 20ug-20F17 Day 7/14
Bleo + 2ug-20F17 Day 7
Bleo + 2ug-20F17 Day 7/14
Bleo + 2ug-NTBYBG Day 7
Bleo + 2ug-NTBYBG Day 7/14

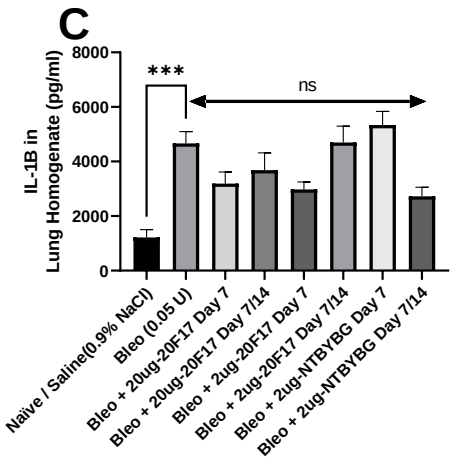
C
IL-1B in Lung Homogenate (pg/ml)
8000
6000
4000
2000
0
***
ns
Naïve / Saline(0.9% NaCl)
Bleo (0.05 U)
Bleo + 20ug-20F17 Day 7
Bleo + 20ug-20F17 Day 7/14
Bleo + 2ug-20F17 Day 7
Bleo + 2ug-20F17 Day 7/14
Bleo + 2ug-NTBYBG Day 7
Bleo + 2ug-NTBYBG Day 7/14

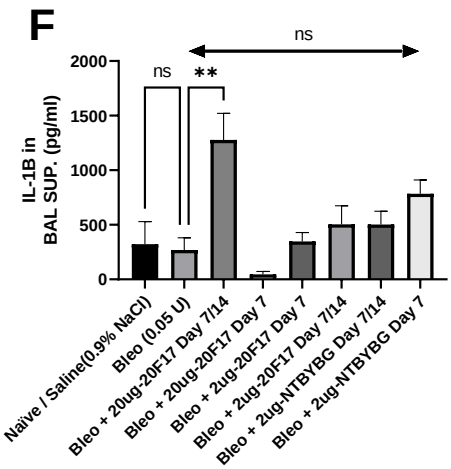
F
IL-1B in BAL SUP. (pg/ml)
2000
1500
1000
500
0
ns
**
ns
Naïve / Saline(0.9% NaCl)
Bleo (0.05 U)
Bleo + 20ug-20F17 Day 7/14
Bleo + 20ug-20F17 Day 7
Bleo + 2ug-20F17 Day 7
Bleo + 2ug-20F17 Day 7/14
Bleo + 2ug-NTBYBG Day 7
Bleo + 2ug-NTBYBG Day 7/14

Figure 20: Cytokine analysis in lung homogenate and BAL supernatant

Total cytokine expression as measured in lung homogenate from right lobes of treated mice and in lung BAL fluid. Bleomycin group has the highest TNF-a, TGFB, and IL-1B expression in lung homogenate. Values for BAL supernatant are markedly lower in comparison to lung homogenate. 20F17 groups have significantly lower TNF-a and TFGB levels in lung homogenate. is significantly lower in 20F17 and NTB-YBG groups relative to the bleomycin control group (B). Bar graphs represent mean ± SEM from 4-5 biological replicates per group, *P < 0.05, ****P < 0.0001. Significance was established using GraphPad, Prism 9.0 with Two-way ANOVA using Tukey's Multiple Comparison Test.

3.3 TMA analysis for collagen and M2 marker quantification

Using TMA technology, we generated mouse TMA 39 with all FFPE left lobe tissues from the animal study on a single paraffin block. The block was serial sectioned and stained for H/E, Masson's Trichrome, PSR, as well as IHC staining for mouse macrophage marker F4/80, M2 markers CD206 and CD163, pSYK, and myofibroblast marker aSMA. A representative image of the staining is shown in Figure 21 A. Collagen content in the parenchyma through Trichrome staining, % CD206+ cells, and % pSYK+ cells have been quantified via HALO as of now (B-D). The % Collagen / Tissue values were generated by omitting the airways and blood vessels from the cores, leaving only the parenchyma. The %+ cells are cells positive for protein divided by the total number of cells in the core. The H-Score which assesses the overall staining intensity for all the cells and gives a value that to give an idea as to the overall expression level of the protein in the tissue was also generated for pSYK and CD206 (Supplementary Figure 24). Parenchymal collagen, a reliable measure of fibrosis, is elevated in the Bleo group relative to the saline group (B). For parenchymal collagen quantification for treatment, groups are not significantly different but there is immense variability which suggests a follow-up with a larger sample size is needed. There seem to be no visible trends and

differences in all groups with % CD206+ and % pSYK+ cells as determined through HALO quantification (C-D).

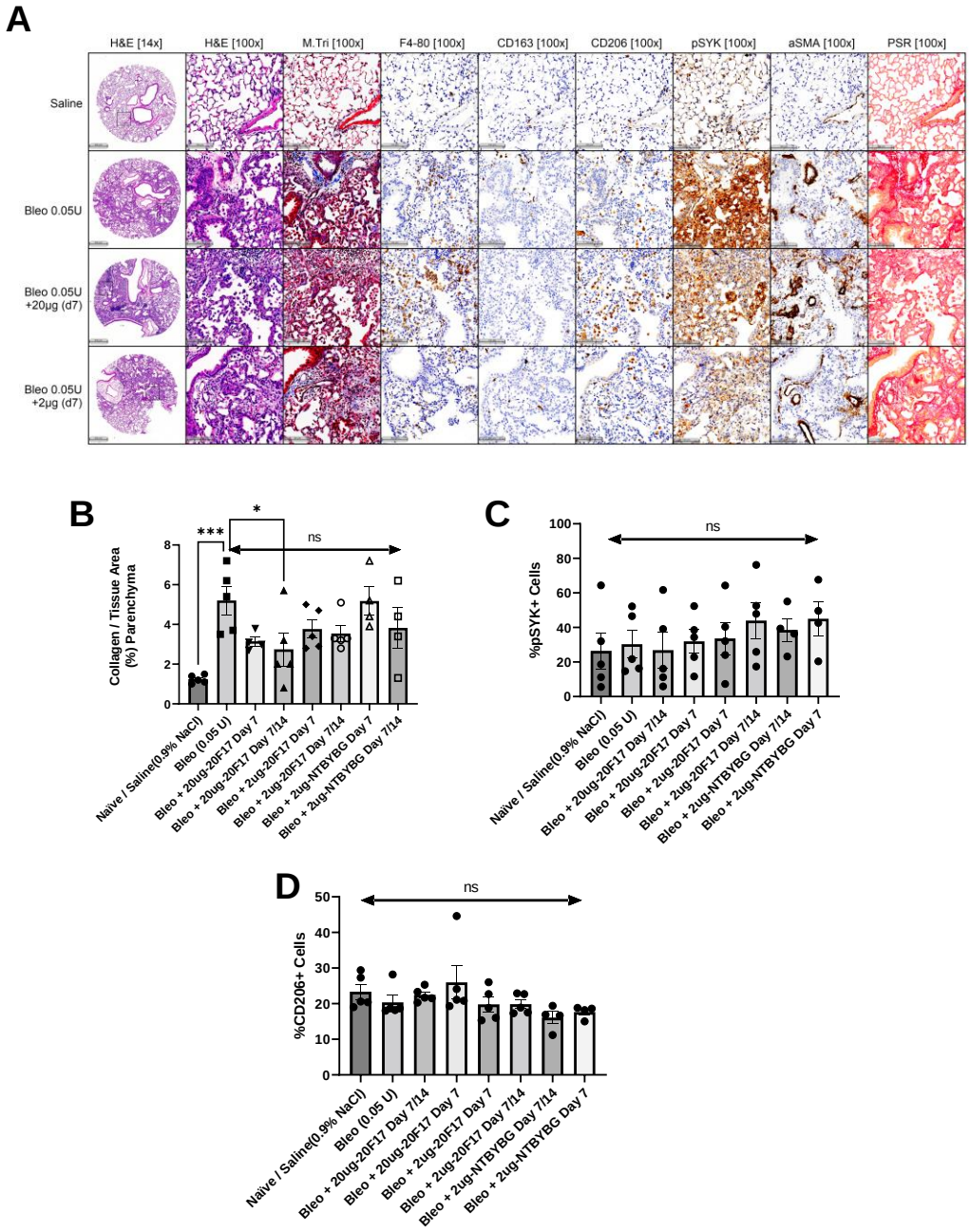

Figure 21: Representative TMA staining and quantification of parenchymal collagen, % CD206+ cells, and %pSYK+ cells

Stained TMA cores were imaged through the Olympus V120 slider scanner, with a subset of study groups shown as a representative image. % Collagen/Tissue in Parenchyma was determined through quantification of the Masson's Trichrome stain (airways and vasculature were omitted) (B). % CD206+ and % pSYK+ cells were determined relative to the total number of cells in the corresponding core (C-D). Bar graphs represent mean ± SEM from 4-5 biological replicates per group, ***$P < 0.001$. Significance was established using GraphPad, Prism 9.0 with One-way ANOVA using Dunnet's Multiple Comparison Test.

DISCUSSION

Profibrotic (M2) macrophages are greatly involved in the wound healing process and are of interest in the context of fibrosis as they can mediate fibroblast proliferation and myofibroblast differentiation (Pesci et al., 2010; T. Wynn & Barron, 2010). Studies have shown that the depletion of macrophages has lead to less severe fibrotic outcomes in models of fibrotic disease (Gibbons et al., 2011; Kim et al., 2015). However, depletion strategies are not a viable option as this can have disastrous effects on the immune environment. Specific targeting of macrophages is a more viable option and specifically, M2 macrophages for their potential activity modulation in fibrosis. Targeting the dectin-1 receptor offers a unique solution to the problem of idiopathic pulmonary fibrosis (IPF).

Being expressed far more abundantly on the surface of M2 macrophages, dectin-1 activation has an immune modulatory effect on M2 macrophages to have them adopt M1-like characteristics (Liu et al., 2015; Patel, 2018). IPF is an immunosuppressive disease and this eventually leads to patient mortality, so it's worth an effort to understand how changing the local immune environment by dectin-1 activation can be beneficial in fibrosis. Using FFPE IPF tissue samples we can see that dectin-1is a suitable target (supplementary figures 25 and 27). It is also clear that dectin-1 is co-localized in IPF tissue with cells expressing CD68, a macrophage marker (supplementary figure 26). Consequently, it is possible to target macrophages in a cell-specific way through the dectin-1 targeting strategy.

This thesis is largely geared around the use of beta-glucan microparticles and how they can be used to influence M2 macrophage activity. Beta-glucan microparticles, with 1-3 glycosidic linkages are a high-affinity ligand for dectin-1 (Brown, 2006; Liu et al., 2015). The initial idea for this thesis was to use beta-glucan microparticles as a loading vehicle to deliver nintedanib to M2 macrophages as inhalable therapeutics for IPF. Ceapro Inc.'s PGX process allows beta-glucan microparticles to have increased porosity and be used as a scaffold for nintedanib impregnation. While NTB-YBG, with a 0.5% by weight loading capacity for nintedanib, is an interesting microparticle to work with as just the vehicle itself can have a beneficial effect by modulating macrophage activity. To achieve 50nM per animal treatment of nintedanib, as used in previous animal studies we would need to administer a dose of approximately 26.95 ug of NTB-YBG. Redesigning the animal experiments with respect to this does would allow us to accurately compare the effect of PGX betaglucan with nintedanib to just nintedanib alone.

Terms such as "reprogramming" or "relearning" are often used in the context of M2 macrophage behavior to suggest functional heterogeneity in these macrophages (T. Wynn & Barron, 2010). Activity modulation in M2 macrophages is an exciting topic as this can be used to influence the local immune environment. To test how beta-glucan microparticles can influence M2 polarization we used two different types of polarization models. In the co-treatment model, beta-glucan and the anti-inflammatory polarization cocktail (IL4/IL13/IL6) are presented to a naive macrophage concurrently. In the polarized model, pre-polarized M2 macrophages are treated with beta-glucan. Polarization was tested by tracking well-established M2 macrophage markers such as

CD206 and arginase-1 (Orecchioni et al., 2019). We found that the effect of beta-glucan on macrophage polarization is dependent upon the timing of the intervention.

20F17, our primary PGX yeast beta-glucan microparticle, effectively inhibited arginase-1 activity in the co-treatment model with wild-type mouse macrophages. This inhibition was dose-dependent, with maximal inhibition occurring at the 100 ug/ml concentration (Figure 7). This is an interesting finding because it suggests that beta-glucan can stop naive macrophages from becoming M2 polarized and causing deleterious profibrotic activity in fibrotic disease. With no discernable cytotoxicity, based on LDH release, 20F17 even at a massive 1000 ug/ml concentration is safe to use (Figure 7B). 20F17 can also inhibit arginase-1 activity with a lower biological variability relative to other beta-glucan varieties at a 100ug/ml concentration (Figure 8). OBG does not inhibit arginase-1 activity to the same level as the other microparticle, this can be since OBG has a mixed 1,3 and 1,4 glycosidic linkage and is itself a soluble polymer which is different from the others' predominantly 1,3 linkage. This seems to suggest that perhaps water insoluble microparticles have an advantage in inhibiting M2 polraization relative to soluble polymers as this process may be uptake-dependent. An experiment that assesss 20F17 uptake versus OBG is a logical next step to assess the mechanism of inhibition. 20F17 inhibits arginase activity equally as well as its non-PGX counterpart YBG, suggesting that PGX processing does not alter 20F17's ability as an M2 inhibitor. Using flow cytometry analysis in the co-treatment model we saw that the CD206 frequency was decreased in both WT and Dectin-1 KO macrophages in a dose-dependent manner, with the 100 ug/ml dose significantly decreasing CD206 positivity (Figure 10). This data

suggests that 20F17 treatment results in the loss of CD206 in cells, even though the % live-cell frequency is not different amongst the treatment groups. The CD206 levels in groups co-treated with 100 ug/ml 20F17 are lower than non-treated M0 controls. This idea needs to be explored further to determine a mechanism for the CD206 loss. From an IPF perspective, this is an excellent avenue of research because soluble CD206 levels are associated with mortality, with higher levels seen in exacerbated IPF cases ((Zou et al., 2020).

In the M2 polarized subset, of mouse wildtype BMDMs, there are no significant changes in arginase-1 activity seen post 24 hours of 20F17 treatment, even when doses from 1 ug/ml to 1000 ug/ml were used (Figure 11A). The arginase-1 activity level in the M2 group was significantly greater than the naive (M0) group through which we know that our assay was set up properly. Accordingly, there are no discernable differences in cell viability associated with 20F17 treatment, based on LDH release (Figure 11 B). Liu et al., in the past, have demonstrated changes at the transcriptomic level in M2-like TAMs (tumor-associated macrophages) after 24 hours of beta-glucan treatment at a dose of 100 ug/ml, suggesting that mRNA transcription of proinflammatory cytokines is upregulated (2015). This seems to suggest that it might take longer than 24 hours for us to seen changes in arginase-1 activity based on how we have set up our model. This is a possible future avenue of research where arginase activity is tracked at 48 and 72 hours of beta-glucan treatment along with LDH release. Assessing the frequency of CD206 cells in the polarized model shows that 20F17 treatment causes a decrease in CD206 expression of polarized M2 macrophages relative to un-treated M2 control and M0 control (Figure 12

B). This decrease is more significant in WT macrophages, with far greater variability in dectin-1 KO macrophages. CD206 itself has been shown to be involved in particle and bacterial phagocytosis, therefore the decrease in expression can be related to increased particle uptake in M2 macrophages (Wollenberg et al., 2002). The lower variability can be dectin-1 dependent as WT-M2 macrophages should have the most dectin-1 activation. For a follow-up experiment tracking pSYK staining in proxy of dectin-1 activation should be considered to show this as a dectin-1 dependent process.

Another key outcome of the polarized model is that we demonstrated that M2 macrophages can adopt M1-like characteristics when treated with 20F17 in a dose and dectin-1 dependent manner. 20F17 intervention in M2 polarized WT macrophages causes increased production of TNF-a and nitrite after 24 hours of treatment (Figure 13). There are no significant changes in nitrite production by KO-M2 macrophages. WT and KO M1 macrophages produce significantly higher TNFa and nitrite relative to M0 controls, with M1 treated with 20F17 showing no further changes relative to M1. This data suggests that while 20F17 causes TNF-a and nitrite expression in WT M2 macrophages, it does not change M1 activity. This may be because M1 macrophages do not express dectin-1 as abundantly as M2 or that functional expression seen in M1 is the biological limit. The role of the dectin-1 receptor is very clear in this process as the KO M2 macrophages did not significantly change in terms of nitrite expression. It is also important to note here that M2 macrophages treated with 20F17 did not display M1 chracteristics to the same level as M1 macrophages, this is beneficial in the context of fibrotic lung disease. Since, M2 macrophages treated with 20F17 do not completely become M1-like we have evidence to

suggest that macrophage triggered inflammatory responses may be avoided. Transcriptomic analysis of M2 macrophages treated with 20F17 would offer more support to the M2 activity modulation experiments. An RNA nano-string code set with M1 and M2 genes could be generated and used to show gene changes caused by 20F17 treatment in polarized M2 cells with dectin-1 KO cells as an interesting control.

The role 20F17 plays in influencing the M2 polarization of THP-1 human macrophages is a little unclear. Tracking CCL18, a potent chemical messenger related to myofibroblast differentiation, is a suitable way to discern human macrophage M2 polarization ((Prasse et al., 2006). 20F17 co-treatment partly inhibits CCl18 production in M2 macrophages, albeit at a high dose of 1000 ug/ml, with a minimal significant decrease relative to the M2 control (Figure 14). To further investigate this it would make sense to test this in human primary macrophages perhaps monocyte-derived. IPF patient monocytes co-treated with 20F17 and the M2-cocktail would be an enlightening follow-up. It is in line with the animal experiments to see that CCL18 levels in the polarized experiments do not change in response to 20F17 treatment but the TNF-a release in treated M2 polarized THP-1 macrophages is also minimal (Figure 15). These findings illustrate the need to explore this idea in a new primary cell model as perhaps the THP-1 immortalized cell line is hard to influence in-vitro.

A possible explanation for the irregular results in the THP-1 cells can be due to uptake. We successfully labeled 20F17 with a robust aniline blue, fluorescent tag (Figure 16). The uptake was much lower in THP-1 cells at 6 hours (less than 3 % uptake) relative to BMDMs. The idea of this experiment was to test whether M2 or M0 macrophages can

uptake 20F17 better. M2 macrophages have higher phagocytosis rates compared to the other types (Kapellos et al., 2016). M0 and M2 macrophages were treated with 10 or 100 ug/ml 20F17 and assessed for uptake at 1 and 6 hours. There were no significant differences with 20F17 uptake within WT and KO macrophages at 1 hour (Figure 17). Uptake was dose-dependent in WT as 100 ug/ml groups display higher uptake relative to 10 ug/ml groups. WT-M2 group treated with 100 ug/ml 20F17 had the highest uptake at 6 hours, significantly higher than the KO-M2 group treated with 100 ug/ml 20F17. This also points towards the dectin-1 dependent action of 20F17 in polarized M2 macrophages. Figure 18 shows that WT-M2 macrophages have the highest staining at 6 hours, this supports the idea that dectin-1 is an important mediator in 20F17 uptake at least the 6-hour mark. The uptake in WT-M2 is still higher at the 6-hour mark compared to the KO-M2. The fact that uptake increases with dose is expected as the more microparticles there are available to macrophages the more more they will uptake. Analyzing uptake at earlier timepoints allows us to determine how much of the initial uptake is dectin-1 related, relative to our knockout model. We predict that this difference may become less prominent at later timepoints given the inherent phagocytic nature of macrophages, especially the M2 variety. Further experimentation that tracks uptake for up to 24 hours can give further clarification as to which macrophage types uptake 20F17 more.

Until this point, it is clear that PGX beta-glucan (20F17) microparticles can modulate polarized M2 macrophage activity in a dectin-1 dependent manner as well as inhibit M2 polarization. Further, we have shown that M2 macrophages uptake 20F17 to a higher degree relative to naïve macrophages, also in a dectin-1 dependent manner. Both these

findings are in line with the hypothesis and make the case for 20F17 as a specific and suitable M2 activity modulator. In regards to 20F17's use as a therapeutic in the bleomycin model of fibrotic lung disease, we first carried out tolerability studies (in naive and diseased mice) with the conclusion that 20F17 was a potent immune modulator and inflammatory at high doses (>20 ug/animal). In the most recent therapeutic experiment, described in this document, we explored the effect of a low dose (2 ug per animal) and a high dose (20 ug per animal) on fibrotic outcomes. With 20F17/NTB-YBG intervention occurring at 7 days post bleomycin intubation and select groups receiving a second intervention at 14 days. Day 7 was chosen as the first intervention time since this is the time where the acute inflammatory phase of the model is nearing completion and the wound healing phase starts. This time is also where we predicted that most of the dectin-1 positive macrophages will be present or accumulating in the lungs. Considering survival rate, 20F17 is well tolerated by mice intubated with bleomycin and only one mouse (20 ug-20F17 at day 7 group) reached endpoint and had to be sacrificed at day 17 out of the 38 mice in the study. Referring to the effect of bleomycin on body weight, we saw that 0.05 units of bleomycin caused a loss of 9-11 % weight by day 7 in all intubated mice meaning that all bleomycin groups were prone to developing fibrosis. (Figure 19). Accordingly, naïve mice given saline did not lose weight. For soluble collagen content in the lung, all groups treated with microparticles had significantly lower collagen amounts in the right lung homogenate relative to the bleomycin control group. Further cytokine assessments in lung homogenate showed a trend where the bleomycin fibrotic control group had the highest total levels of TNF-a, TGFB, and IL-1B (Figure 20). TGFB levels

were decreased in all treatment groups relative to the bleomycin group which is beneficial as microparticle treatment seems to be decreasing it. It would have been in line with the in-vitro assessments to see pro-inflammatory cytokines TNF-a and IL-1B to be elevated in the microparticle treatment groups, but perhaps the timing is the reason. Spikes in proinflammatory cytokine release in monocytes treated with beta-glucan are seen within the first 8 hours of treatment (Abel & CzoP, n.d.). Therefore, to pick up changes in pro-inflammatory cytokine release biological samples would need to be collected much earlier rather than waiting until day 21. It seems that microparticle treatment downregulates cytokine expression at day 21 and this is carried over in the bronchioloalveolar lavage (BAL) supernatant, which shows no significant differences in cytokine expression in all groups. This downregulation or return to normal (relative to untreated saline group) of cytokine exoression is inline with other evidence that the immune modulatory effects of these PGX microparticles are indeed shortlived.

Histology data from mouse TMA 39 gives some puzzling results as well, but the staining remains largely unquantified. Our next steps would be to consult a pathologist to determine the immune cell differences in the H/E slides. % Collagen content in the parenchyma, while insignificant, shows large variations in the treatment groups relative to the bleomycin group (Figure 21). Interestingly, the 20 ug dose of 20F17 given at both day 7 and 14 seems to be beneficial in causing a decrease in collagen content. This shows that perhaps a higher dose given at a higher frequency is more beneficial in dampeneing fibrotic progression in the bleomycin model. % CD206+ and pSYK cells also show no significant differences amongst all the groups, we would need to quantify CD163 and

F4/80 and macrophage markers to see if a difference exists there. It would be hard to conclude on the efficacy of 20F17 as an anti-fibrotic therapeutic since further experimentation is needed.

Building upon the evidence seen in both the cell culture as well as the animal experiment we see that there is legitimate potential for PGX beta-glucan or 20F17 to be an anti-fibrotic agent. We have verified our results relating to the effect 20F17 has on M2 macrophages which show that it works by essentially reprogramming these cells to be less profibrotic. Reprogramming M2 macrophages prevents release of cytokines that initate collage and extracellular matrix deposition, which can lead to fibrosis supression. This idea is seen in the results of the bleomycin experiment where we saw decreased TGF-B and proinflammatory cytokine release in the lung and lowered collagen content at the 20ug dose given at day 7 and 14. Based on these finidigs it is not implausible that an experimentally determined dose(s) of 20F17 can be similarly used to suppress fibrosis in patients with IPF as well as other fibrotic diseases. As such it is pertinent to eventually test 20F17 in validated models of human fibrotic lung disease.

Timing of the 20F17 intervention, 20F17 intervention dose, and the use of 20F17 in a prophylactic study are a few key considerations for the next iteration of this work. We would need to run a characterization study to see M2 macrophage and dectin-1 expression at days 7, 9, and 11 of the bleomycin model to see what is a suitable time point of intervention. The time day 7 timepoint is perhaps too early as we could be adding an inflammatory agent on top of already injured tissue. We have established that 20F17 works on macrophages in a dose-dependent manner. It is also important to establish an in-

vivo dose where we do not cause an inflammatory response with a high dose or no response with a low dose. Consultation with a pathologist on the current TMA as well as the pending BAL immune cell analysis would allow us to make judgments on a suitable dose closer to either 2 ug or 20 ug as well as frequency. Setting up a prophylactic study with 20F17 would be an interesting next step as we could determine if beta-glucan microparticles can prevent fibrosis onset, as was seen in rats given beta-glucan orally before bleomycin intubation (Iraz et al., n.d.). The drug-loaded beta-glucans should also be revisited and independently assessed in subsequent experiments. The NTB-YBG microparticles were not significantly different than 20F17 in the animal experiment, but perhaps a higher drug loading capacity or more frequent low dose treatments might be more beneficial.

20F17 influences dectin-1 expressing M2 macrophages. The most pressing next steps would be to gain mechanistic insight into this phenomenon. Analysis of the gene signature of WT-M2 in comparison to dectin-1 KO-M2 macrophages post a 20F17 treatment would provide a clearer picture of the importance of the dectin-1 receptor. Metabolic assessment of M2 macrophages and how it changes with 20F17 treatment would also be an interesting option. There is immense potential for 20F17 to be effective as an immune modulator and it is a valid compound to be studied as a fibrosis therapeutic.

SUPPLEMENTARY FIGURES

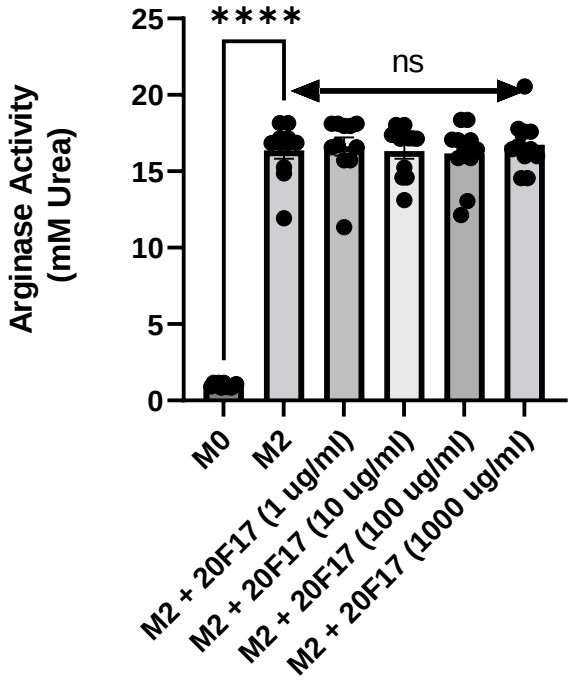

Supplementary Figure 22: (Pooled Experiment) Polarized M2 macrophages (24 hours IL-4/IL-13/IL-6) treated with 20F17 (1 ug to 1000 ug /ml) do not show decreases in arginase-1 activity

Arginase-1 activity is significantly increased in M2 treated wildtype BMDMs relative to naïve (M0) control and is not significantly different in the 20F17 treatment groups. Three separate polarized model experiments were pooled and normalized relative to M0 values for each set. Bar graphs represent mean ± SEM from biological replicates per group, ****$p < 0.0001$, $n = 11$. Significance was established using GraphPad, Prism 9.0 with Two-way ANOVA using Tukey's Multiple Comparison Test.

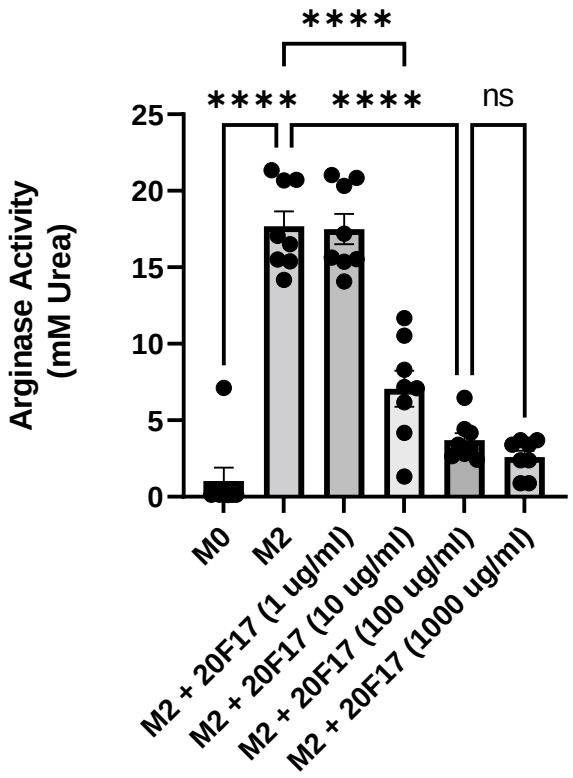

Supplementary Figure 23: (Pooled Experiment) Examining arginase-1 activity in naive macrophages treated with M2 cocktail and 20F17

Beta-glucan (20F17) intervention in a co-treatment M2 polarization assay with WT BMDMs yields differences in arginase-1 activity relative to beta-glucan concentration at 24 hours of treatment. 20F17 and IL-4/IL-13/IL-6 co-treatment show significant inhibition of arginase-1 production starting at the 10 ug/ml concentration. 2 independent experiments were pooled and normalized relative to their respective M0 group. Bar graphs represent mean ± SEM from 8 biological replicates per group, ****$p < 0.0001$, $n = 8$. Significance was established using GraphPad, Prism 9.0 with Two-way ANOVA using Tukey's Multiple Comparison Test.

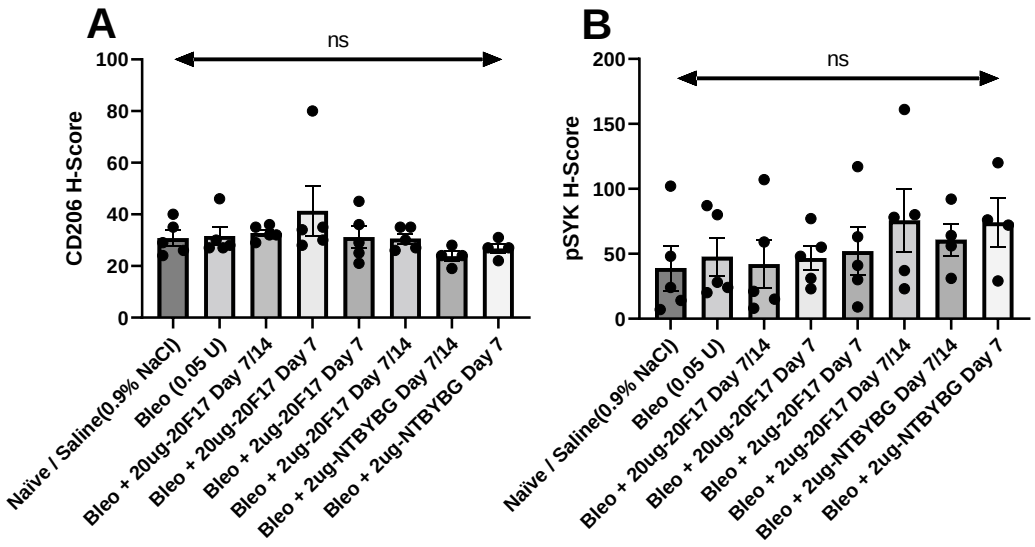

Supplementary Figure 24: H-Scores for CD206 and pSYK for IHC staining of mouse TMA 39

No significant differences are seen. Bar graphs represent mean ± SEM from 4-5 biological replicates per group. Significance was established using GraphPad, Prism 9.0 with Two-way ANOVA using Tukey's Multiple Comparison Test.

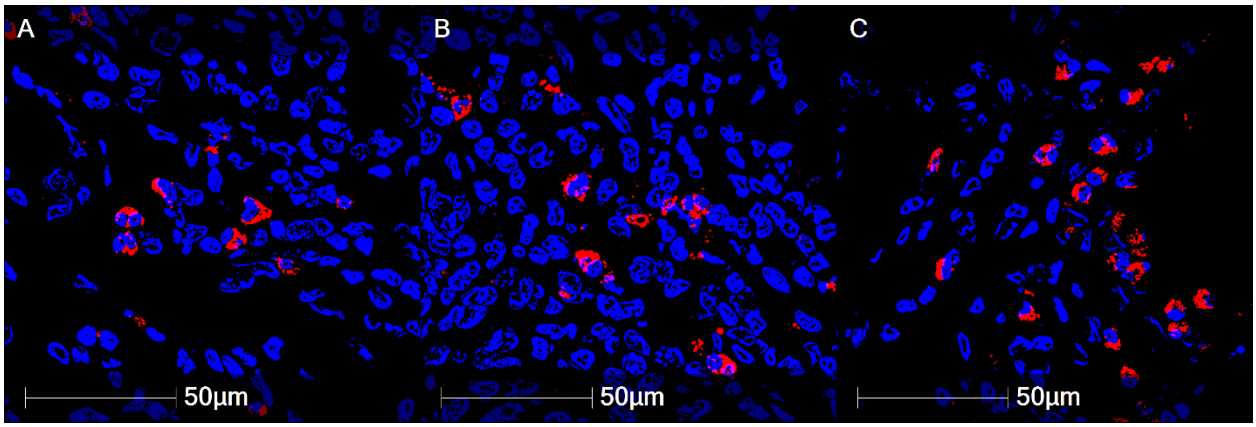

Supplementary Figure 25: Dectin-1 expression visualization through fluorescent in-situ hybridization and detection in HALO™. Dectin-1 is detected with the Texas Red fluorochrome with DAPI counterstain in IPF tissue.

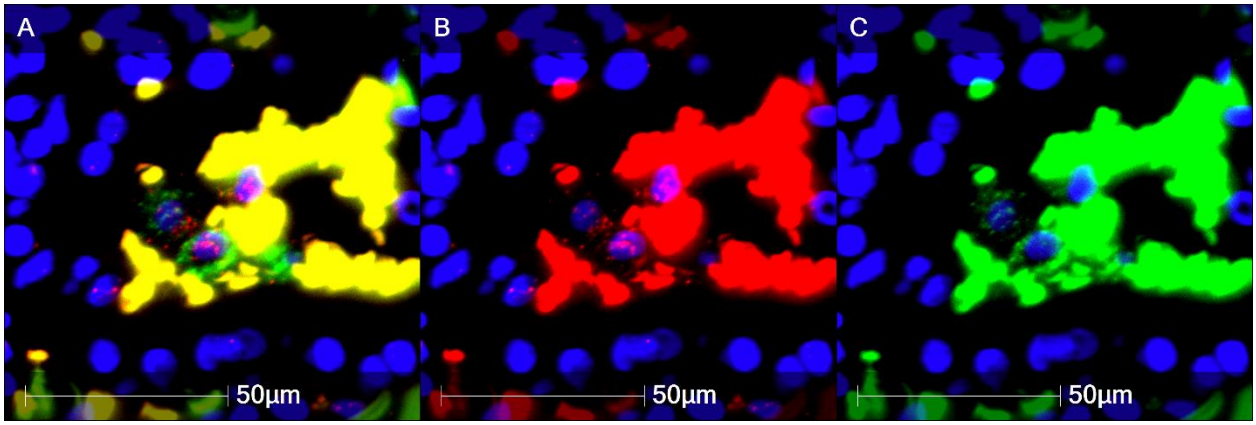

Supplementary Figure 26: Colocalization of Dectin-1 and CD68 using RNAscope® duplex fluorescent in-situ hybridization and detection in HALO™ in IPF tissue.

Dectin-1 is detected with the Texas Red fluorochrome on Channel 1 and CD68 is detected with the FITC fluorochrome on Channel 2. Dual-positive cells are detected using the fluorescent in-situ hybridization module in HALO™.

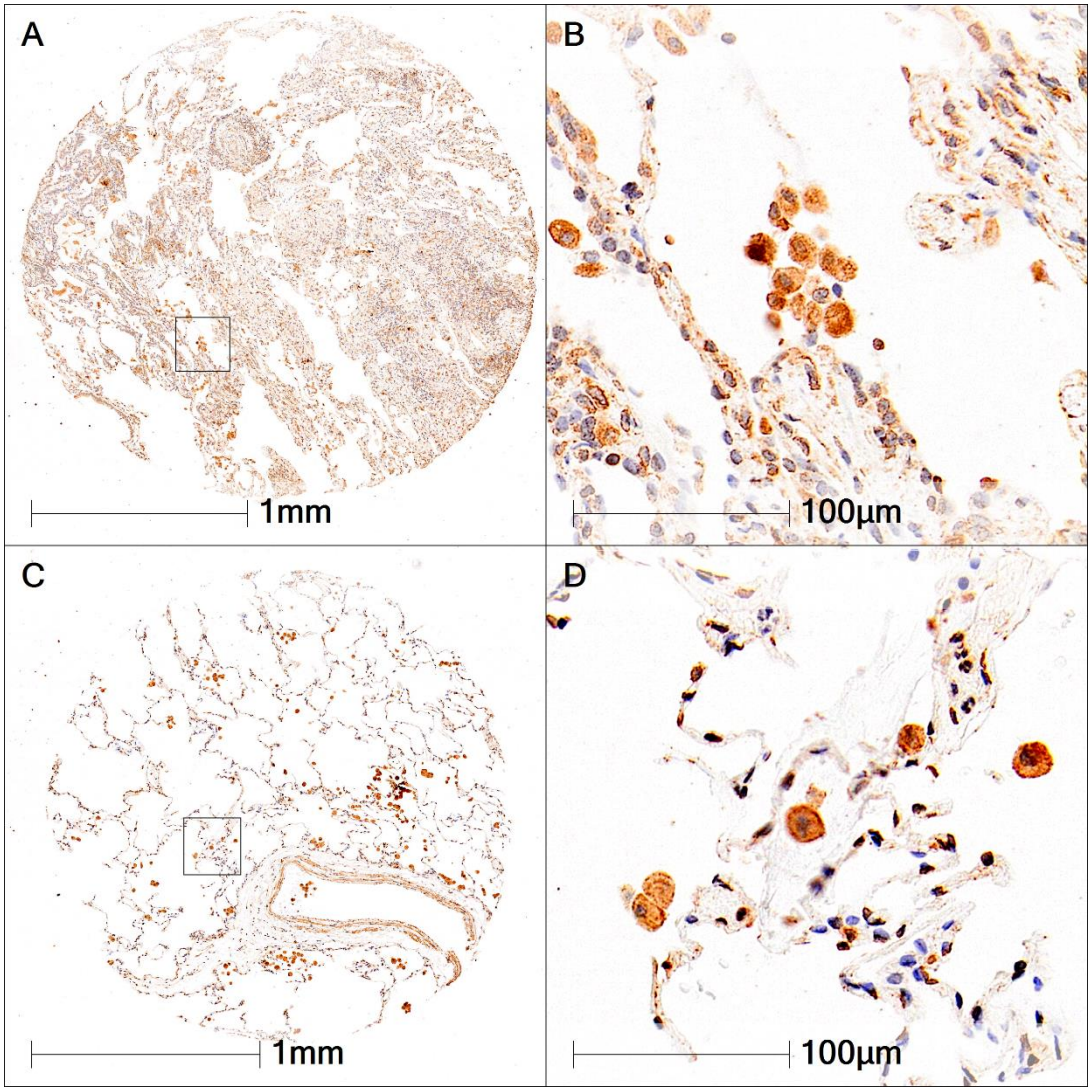

Supplementary Figure 27: Dectin-1 expression is more prominent in IPF tissue

Dectin-1 expression is more prominent in IPF tissue (A-B) relative to normal control tissue (C-D). Immunohistochemical stain for Dectin-1 was performed on serial sections of a TMA and used to assess expression.

REFERENCES

Abed, S., Turner, R., Serniuck, N., Tat, V., Naiel, S., Hayat, A., Mekhael, O., Vierhout, M., Ask, K., & Rullo, A. F. (2021). Cell-specific drug targeting in the lung. *Biochemical Pharmacology*, *190*, 114577. https://doi.org/10.1016/j.bcp.2021.114577

Ayaub, E. A., Dubey, A., Imani, J., Botelho, F., Kolb, M. R. J., Richards, C. D., & Ask, K. (2017). Overexpression of OSM and IL-6 impacts the polarization of pro-fibrotic macrophages and the development of bleomycin-induced lung fibrosis. *Scientific Reports*, *7*(1), 13281. https://doi.org/10.1038/s41598-017-13511-z

Braga, T. T., Agudelo, J. S. H., & Camara, N. O. S. (2015). Macrophages During the Fibrotic Process: M2 as Friend and Foe. *Frontiers in Immunology*, *6*. https://doi.org/10.3389/fimmu.2015.00602

Brown, G. D. (2006). Dectin-1: A signalling non-TLR pattern-recognition receptor. *Nature Reviews Immunology*, *6*(1), 33–43. https://doi.org/10.1038/nri1745

Brown, J., O'Callaghan, C. A., Marshall, A. S. J., Gilbert, R. J. C., Siebold, C., Gordon, S., Brown, G. D., & Jones, E. Y. (2007). Structure of the fungal β-glucan-binding immune receptor dectin-1: Implications for function. *Protein Science*, *16*(6), 1042–1052. https://doi.org/10.1110/ps.072791207

ChÃ¡vez-GalÃ¡n, L., Olleros, M. L., Vesin, D., & Garcia, I. (2015). Much More than M1 and M2 Macrophages, There are also CD169+ and TCR+ Macrophages. *Frontiers in Immunology*, *6*. https://doi.org/10.3389/fimmu.2015.00263

Chen, C.-H., Lin, H.-C., Wang, Y.-H., Wang, C.-Y., Lin, Y. S., & Lai, C.-C. (2021). The

safety of nintedanib for the treatment of interstitial lung disease: A systematic review and meta-analysis of randomized controlled trials. *PLOS ONE*, *16*(5), e0251636. https://doi.org/10.1371/journal.pone.0251636

Desai, O., Winkler, J., Minasyan, M., & Herzog, E. L. (2018). The Role of Immune and Inflammatory Cells in Idiopathic Pulmonary Fibrosis. *Frontiers in Medicine*, *5*, 43. https://doi.org/10.3389/fmed.2018.00043

Epstein-Shochet, G., Pham, S., Beck, S., Naiel, S., Mekhael, O., Revill, S., Hayat, A., Vierhout, M., Bardestein-Wald, B., Shitrit, D., Ask, K., Montgomery, A. B., Kolb, M. R., & Surber, M. W. (2020). Inhalation: A means to explore and optimize nintedanib's pharmacokinetic/pharmacodynamic relationship. *Pulmonary Pharmacology & Therapeutics*, *63*, 101933. https://doi.org/10.1016/j.pupt.2020.101933

Fernandez, I. E., & Eickelberg, O. (2012). The Impact of TGF-β on Lung Fibrosis: From Targeting to Biomarkers. *Proceedings of the American Thoracic Society*, *9*(3), 111–116. https://doi.org/10.1513/pats.201203-023AW

Flaherty, K. R., Wells, A. U., Cottin, V., Devaraj, A., Walsh, S. L. F., Inoue, Y., Richeldi, L., Kolb, M., Tetzlaff, K., Stowasser, S., Coeck, C., Clerisme-Beaty, E., Rosenstock, B., Quaresma, M., Haeufel, T., Goeldner, R.-G., Schlenker-Herceg, R., & Brown, K. K. (2019). Nintedanib in Progressive Fibrosing Interstitial Lung Diseases. *New England Journal of Medicine*, *381*(18), 1718–1727. https://doi.org/10.1056/NEJMoa1908681

Fois, A. G., Sotgiu, E., Scano, V., Negri, S., Mellino, S., Zinellu, E., Pirina, P., Pintus, G.,

Carru, C., Mangoni, A. A., & Zinellu, A. (2020). Effects of Pirfenidone and Nintedanib on Markers of Systemic Oxidative Stress and Inflammation in Patients with Idiopathic Pulmonary Fibrosis: A Preliminary Report. *Antioxidants*, *9*(11), 1064. https://doi.org/10.3390/antiox9111064

Gibbons, M. A., MacKinnon, A. C., Ramachandran, P., Dhaliwal, K., Duffin, R., Phythian-Adams, A. T., van Rooijen, N., Haslett, C., Howie, S. E., Simpson, A. J., Hirani, N., Gauldie, J., Iredale, J. P., Sethi, T., & Forbes, S. J. (2011). Ly6C ^{hi} Monocytes Direct Alternatively Activated Profibrotic Macrophage Regulation of Lung Fibrosis. *American Journal of Respiratory and Critical Care Medicine*, *184*(5), 569–581. https://doi.org/10.1164/rccm.201010-1719OC

Gifford, A. H., Matsuoka, M., Ghoda, L. Y., Homer, R. J., & Enelow, R. I. (2012). Chronic inflammation and lung fibrosis: Pleotropic syndromes but limited distinct phenotypes. *Mucosal Immunology*, *5*(5), 480–484. https://doi.org/10.1038/mi.2012.68

Gross, T. J., & Hunninghake, G. W. (2001). Idiopathic Pulmonary Fibrosis. *The New England Journal of Medicine*, 9.

Iraz, M., Bilgic, S., Samdanci, E., Ozerol, E., Tanbek, K., & Iraz, M. (n.d.). *Preventive and early therapeutic effects of β-Glucan on the bleomycin-induced lung fibrosis in rats*. 12.

Kaja, S., Payne, A. J., Naumchuk, Y., & Koulen, P. (2017). Quantification of Lactate Dehydrogenase for Cell Viability Testing Using Cell Lines and Primary Cultured Astrocytes. *Current Protocols in Toxicology*, *72*(1).

https://doi.org/10.1002/cptx.21

Kalchiem-Dekel, O., Galvin, J., Burke, A., Atamas, S., & Todd, N. (2018). Interstitial Lung Disease and Pulmonary Fibrosis: A Practical Approach for General Medicine Physicians with Focus on the Medical History. *Journal of Clinical Medicine*, *7*(12), 476. https://doi.org/10.3390/jcm7120476

Kapellos, T. S., Taylor, L., Lee, H., Cowley, S. A., James, W. S., Iqbal, A. J., & Greaves, D. R. (2016). A novel real time imaging platform to quantify macrophage phagocytosis. *Biochemical Pharmacology*, *116*, 107–119. https://doi.org/10.1016/j.bcp.2016.07.011

Kim, M. G., Kim, S. C., Ko, Y. S., Lee, H. Y., Jo, S. K., & Cho, W. (2015). The Role of M2 Macrophages in the Progression of Chronic Kidney Disease following Acute Kidney Injury. PLoS One, 10(12), e0143961. doi: 10.1371/journal.pone.0143961

Kimura, Y., Chihara, K., Honjoh, C., Takeuchi, K., Yamauchi, S., Yoshiki, H., Fujieda, S., & Sada, K. (2014). Dectin-1-mediated Signaling Leads to Characteristic Gene Expressions and Cytokine Secretion via Spleen Tyrosine Kinase (Syk) in Rat Mast Cells. *Journal of Biological Chemistry*, *289*(45), 31565–31575. https://doi.org/10.1074/jbc.M114.581322

King, T. E., Pardo, A., & Selman, M. (2011). Idiopathic pulmonary fibrosis. *The Lancet*, *378*(9807), 1949–1961. https://doi.org/10.1016/S0140-6736(11)60052-4

Kolb, M., Bonella, F., & Wollin, L. (2017). Therapeutic targets in idiopathic pulmonary fibrosis. *Respiratory Medicine*, *131*, 49–57. https://doi.org/10.1016/j.rmed.2017.07.062

Lancaster, L. H., de Andrade, J. A., Zibrak, J. D., Padilla, M. L., Albera, C., Nathan, S. D., Wijsenbeek, M. S., Stauffer, J. L., Kirchgaessler, K.-U., & Costabel, U. (2017). Pirfenidone safety and adverse event management in idiopathic pulmonary fibrosis. *European Respiratory Review*, *26*(146), 170057. https://doi.org/10.1183/16000617.0057-2017

Liu, M., Luo, F., Ding, C., Albeituni, S., Hu, X., Ma, Y., Cai, Y., McNally, L., Sanders, M. A., Jain, D., Kloecker, G., Bousamra, M., Zhang, H., Higashi, R. M., Lane, A. N., Fan, T. W.-M., & Yan, J. (2015). Dectin-1 Activation by a Natural Product β-Glucan Converts Immunosuppressive Macrophages into an M1-like Phenotype. *The Journal of Immunology*, *195*(10), 5055–5065. https://doi.org/10.4049/jimmunol.1501158

Moeller, A., Ask, K., Warburton, D., Gauldie, J., & Kolb, M. (2008). The bleomycin animal model: A useful tool to investigate treatment options for idiopathic pulmonary fibrosis? *The International Journal of Biochemistry & Cell Biology*, *40*(3), 362–382. https://doi.org/10.1016/j.biocel.2007.08.011

Murray, P. J., & Wynn, T. A. (2011). Protective and pathogenic functions of macrophage subsets. *Nature Reviews Immunology*, *11*(11), 723–737. https://doi.org/10.1038/nri3073

Okada, H., & Ohya, Y. (2016). Fluorescent Labeling of Yeast Cell Wall Components. *Cold Spring Harbor Protocols*, *2016*(8), pdb.prot085241. https://doi.org/10.1101/pdb.prot085241

Orecchioni, M., Ghosheh, Y., Pramod, A. B., & Ley, K. (2019). Macrophage

Polarization: Different Gene Signatures in M1(LPS+) vs. Classically and M2(LPS–) vs. Alternatively Activated Macrophages. *Frontiers in Immunology*, *10*, 1084. https://doi.org/10.3389/fimmu.2019.01084

Park, S., & Lee, E. J. (2013). Recent Advances in Idiopathic Pulmonary Fibrosis. *Tuberculosis and Respiratory Diseases*, *74*(1), 1. https://doi.org/10.4046/trd.2013.74.1.1

Patel, H. (2018). INVESTIGATING THE ROLE OF DECTIN-1 AS A MARKER OF PROFIBROTIC MACROPHAGES IN THE PROGRESSION OF PULMONARY FIBROSIS. *Medical Sciences*, 67.

Prasse, A., Pechkovsky, D. V., Toews, G. B., Jungraithmayr, W., Kollert, F., Goldmann, T., Vollmer, E., Müller-Quernheim, J., & Zissel, G. (2006). A Vicious Circle of Alveolar Macrophages and Fibroblasts Perpetuates Pulmonary Fibrosis via CCL18. *American Journal of Respiratory and Critical Care Medicine*, *173*(7), 781–792. https://doi.org/10.1164/rccm.200509-1518OC

Qie, Y., Yuan, H., von Roemeling, C. A., Chen, Y., Liu, X., Shih, K. D., Knight, J. A., Tun, H. W., Wharen, R. E., Jiang, W., & Kim, B. Y. S. (2016). Surface modification of nanoparticles enables selective evasion of phagocytic clearance by distinct macrophage phenotypes. *Scientific Reports*, *6*(1), 26269. https://doi.org/10.1038/srep26269

Raghu, G., Remy-Jardin, M., Myers, J. L., Richeldi, L., Ryerson, C. J., Lederer, D. J., Behr, J., Cottin, V., Danoff, S. K., Morell, F., Flaherty, K. R., Wells, A., Martinez, F. J., Azuma, A., Bice, T. J., Bouros, D., Brown, K. K., Collard, H. R., Duggal,

A., … Wilson, K. C. (2018). Diagnosis of Idiopathic Pulmonary Fibrosis. An Official ATS/ERS/JRS/ALAT Clinical Practice Guideline. *American Journal of Respiratory and Critical Care Medicine*, *198*(5), e44–e68. https://doi.org/10.1164/rccm.201807-1255ST

Roedel, E. Q., Cafasso, D. E., Lee, K. W. M., & Pierce, L. M. (2012). Pulmonary toxicity after exposure to military-relevant heavy metal tungsten alloy particles. *Toxicology and Applied Pharmacology*, *259*(1), 74–86. https://doi.org/10.1016/j.taap.2011.12.008

Sica, A., & Mantovani, A. (2012). Macrophage plasticity and polarization: In vivo veritas. *Journal of Clinical Investigation*, *122*(3), 787–795. https://doi.org/10.1172/JCI59643

Somogyi, V., Chaudhuri, N., Torrisi, S. E., Kahn, N., Müller, V., & Kreuter, M. (2019). The therapy of idiopathic pulmonary fibrosis: What is next? *European Respiratory Review*, *28*(153), 190021. https://doi.org/10.1183/16000617.0021-2019

Tanjore, H., Blackwell, T. S., & Lawson, W. E. (2012). Emerging evidence for endoplasmic reticulum stress in the pathogenesis of idiopathic pulmonary fibrosis. *American Journal of Physiology-Lung Cellular and Molecular Physiology*, *302*(8), L721–L729. https://doi.org/10.1152/ajplung.00410.2011

Wei, J., Rahman, S., Ayaub, E. A., Dickhout, J. G., & Ask, K. (2013). Protein Misfolding and Endoplasmic Reticulum Stress in Chronic Lung Disease. *Chest*, *143*(4), 1098–1105. https://doi.org/10.1378/chest.12-2133

Weischenfeldt, J., & Porse, B. (2008). Bone Marrow-Derived Macrophages (BMM): Isolation and Applications. *Cold Spring Harbor Protocols*, *2008*(12), pdb.prot5080-pdb.prot5080. https://doi.org/10.1101/pdb.prot5080

Willcocks, S., Yamakawa, Y., Stalker, A., Coffey, T. J., Goldammer, T., & Werling, D. (2006). Identification and gene expression of the bovine C-type lectin Dectin-1. *Veterinary Immunology and Immunopathology*, *113*(1–2), 234–242. https://doi.org/10.1016/j.vetimm.2006.04.007

Wollin, S. L., Bonella, F., & Stowasser, S. (2015). Idiopathic pulmonary fibrosis: Current treatment options and critical appraisal of nintedanib. *Drug Design, Development and Therapy*, 6407. https://doi.org/10.2147/DDDT.S76648

Wood, P. J., & Fulcher, R. G. (1984). Specific interaction of aniline blue with (1 → 3)-β-d-glucan. *Carbohydrate Polymers*, *4*(1), 49–72. https://doi.org/10.1016/0144-8617(84)90044-4

Wynn, T. A. (2004). Fibrotic disease and the TH1/TH2 paradigm. *Nature Reviews Immunology*, *4*(8), 583–594. https://doi.org/10.1038/nri1412

Wynn, T. A., & Vannella, K. M. (2016). Macrophages in Tissue Repair, Regeneration, and Fibrosis. *Immunity*, *44*(3), 450–462. https://doi.org/10.1016/j.immuni.2016.02.015

Wynn, T., & Barron, L. (2010). Macrophages: Master Regulators of Inflammation and Fibrosis. *Seminars in Liver Disease*, *30*(03), 245–257. https://doi.org/10.1055/s-0030-1255354

Yu, E., Goto, M., Ueta, H., Kitazawa, Y., Sawanobori, Y., Kariya, T., Sasaki, M., &

Matsuno, K. (2016). Expression of area-specific M2-macrophage phenotype by recruited rat monocytes in duct-ligation pancreatitis. *Histochemistry and Cell Biology*, *145*(6), 659–673. https://doi.org/10.1007/s00418-016-1406-y

Zajd, C. M., Ziemba, A. M., Miralles, G. M., Nguyen, T., Feustel, P. J., Dunn, S. M., Gilbert, R. J., & Lennartz, M. R. (2020). Bone Marrow-Derived and Elicited Peritoneal Macrophages Are Not Created Equal: The Questions Asked Dictate the Cell Type Used. *Frontiers in Immunology*, *11*, 269. https://doi.org/10.3389/fimmu.2020.00269

Zhang, F., Ayaub, E. A., Wang, B., Puchulu-Campanella, E., Li, Y., Hettiarachchi, S. U., Lindeman, S. D., Luo, Q., Rout, S., Srinivasarao, M., Cox, A., Tsoyi, K., Nickerson-Nutter, C., Rosas, I. O., & Low, P. S. (2020). Reprogramming of profibrotic macrophages for treatment of bleomycin-induced pulmonary fibrosis. *EMBO Molecular Medicine*, *12*(8). https://doi.org/10.15252/emmm.202012034

Zou, R., Gui, X., Zhang, J., Tian, Y., Liu, X., Tian, M., Chen, T., Wu, H., Chen, J., Dai, J., & Cai, H. (2020). Association of serum macrophage-mannose receptor CD206 with mortality in idiopathic pulmonary fibrosis. *International Immunopharmacology*, *86*, 106732. https://doi.org/10.1016/j.intimp.2020.106732